



A multi-sourced assessment of the spatio-temporal dynamic of soil saturation in the MARINE flash flood model

Judith Eeckman¹, H el ene Roux¹, Audrey Douinot², Bertrand Bonan³, and Cl ement Alberge^{3,4}

¹Institut de M ecanique des Fluides de Toulouse (IMFT), Universit e de Toulouse, CNRS - Toulouse, FRANCE

²Luxembourg Institute of Science and technology, ERIN, Luxembourg

³CNRM, Universit e de Toulouse, M et eo-France, CNRS, Toulouse, France

⁴now at European Space Agency Climate Office, ECSAT, Harwell Campus, Didcot, Oxfordshire, UK

Correspondence: Eeckman Judith ju.eeckman@gmail.com

Abstract. The MARINE hydrological model is a distributed model dedicated to flash flood simulation. Recent developments of the MARINE model are exploited in this work: on the one hand, formerly relying on water height, transfers of water through the subsurface now take place in a homogeneous soil column based on the volumetric soil water content (SSF model). On the other hand, the soil column is divided into two layers, which represent respectively the upper soil layer and the deep weathered rocks (SSF-DWF model). The aim of the present work is to assess the performances of these new representations for the simulation of soil saturation during flash flood events. An exploration of the various products available in the literature for soil moisture estimation is performed. The performances of the models are estimated with respect to several soil moisture products, either at the local scale or spatially extended: i) The gridded soil moisture product provided by the operational modeling chain SAFRAN-ISBA-MODCOU; ii) The gridded soil moisture product provided by the LDAS-Monde assimilation chain, based on the ISBA-a-gs land surface model and assimilating satellite derived data; iii) the upper soil moisture hourly measurements taken from the SMOSMANIA observation network; iv) The Soil Water Index provided by the Copernicus Global Land Service (CGLS), derived from Sentinel1/C-band SAR and ASCAT satellite data. The case study is performed over two French Mediterranean catchments impacted by flash flood events over the 2017-2019 period. The local comparison of the MARINE outputs with the SMOSMANIA measurements, as well as the comparison at the basin scale of the MARINE outputs with the gridded LDAS-Monde and CGLS data lead to the same conclusions: both the dynamics and the amplitudes of the soil moisture simulated with the SSF and SSF-DWF models are better correlated with both the SMOSMANIA measurements and the LDAS-Monde data than the outputs of the base model. The opportunity of improving the two-layers model calibration is then discussed. In conclusion, the developments presented for the representation of subsurface flow in the MARINE model enhance the soil moisture simulation during flash floods, with respect to both gridded data and local soil moisture measurements.

20 1 Introduction

The risk associated with flash flood events is of growing importance, in particular in the Mediterranean area (Payrastr e et al., 2011; Ruin et al., 2014; Su arez-Almi ana et al., 2019). Since extreme precipitation events are expected, with good confidence, to increase both in frequency and in amplitude in the context of a changing climate (IPCC, 2014), the performances of the



modeling tools available for operational purposes are of increasing stake. The main variable of interest for flood simulations at
25 the catchment scale is usually the integrative discharge variable. However, surface runoff, itself controlled by soil infiltration
rates, is shown to exacerbate both human and material risks during extreme events (Vincendon et al., 2010). The representation
of soil processes in the models is thus a key factor for flash flood simulation (Berthet et al., 2009).

Among the variety of models developed for flash flood simulation, a large panel of formalism is applied to model the sub-
30 surface, from no consideration of infiltration flows (Berthet, 2010), to reservoir-like representations of the subsurface or to
detailed parametrizations of the soil physics. In reservoir-like representations, vertical flows can be parametrized through simple
calibrated relations, in particular through linear relations (Perrin et al., 2003), or exponential relations. Other approaches
apply a more physically-oriented representation of infiltration in the subsurface based on the Richard's equation. In this case,
the controlling coefficients are whether calibrated (Roux et al., 2011) or extracted from pedological and geological descriptions
35 (Bouilloud et al., 2010; Vincendon et al., 2010; Vannier et al., 2014).

This variety of models applied for subsurface representation reveals large uncertainties for the quantification of the trans-
fers through the subsurface during flood events. Various works quantify the sensitivity of different models to the subsur-
face parametrization (Tramblay et al., 2010; Garambois et al., 2015; Douinot et al., 2017; Edouard et al., 2018; Lovat et al.,
40 2019). They show that the uncertainties on the processes in the subsurface have a strong impact on both the discharge and the
surface runoff simulation during the flood events. However, the validation of simulated outputs is made hazardous by both
the lack of soil and deep ground description and by the lack of underground flows measurements (Manus et al., 2009). In
this work, an exploration of the various products available in the literature for soil moisture estimation is performed. Three
main types of data can be used to estimate the performances of event-based hydrological models regarding the soil moisture: i)
45 local ground measurements provide locally accurate estimations of soil moisture at shallow depths. The difficulty in comparing
ground measurements to simulation outputs stands in the fact that point measurements do not provide any spatially extended
information. In particular, the SMOSMANIA network (Calvet et al., 2007; Albergel et al., 2009; Parrens et al., 2012) consists
in 21 ground point measurements in Southern France ; ii) continuous models provide gridded information over a large area and
they can provide information for different depths and different variables. However, model outputs are necessarily biased by
50 structural uncertainties of the model and uncertainties on model input. For example, the SAFRAN-ISBA-MODCOU modelling
chain (Habets et al., 2008) as well as the LDAS-Monde products (Albergel et al., 2017) are both based on the ISBA surface
scheme (Noilhan and Planton, 1989; Noilhan and Mahfouf, 1996), implemented in the SURFEX platform (Masson et al.,
2013); iii) Satellite imagery provides valuable spatially extended data. However, remote sensors are able to capture only super-
ficial reflectance of surfaces. Microwave remote sensing (RS) provides a means to quantitatively describe the water content of
55 a shallow near-surface soil layer. However, the variable of interest for applications in short- and medium-range meteorological
modelling and hydrological studies over vegetated areas is the root-zone soil moisture (RZSM) content, which controls plant
transpiration but is not directly observable from space. Since the near-surface soil moisture (SM) is related to RZSM through
diffusion processes, assimilation algorithms may allow its retrieval. Estimation of RZSM from intermittent remotely sensed



60 surface SM data had focused on the assimilation of such data into land surface models. Many studies now also suggest that
constraining those LSMs using various types of earth observations, including vegetation related earth observations, may lead
to a better representation of the RZSM.

The MARINE model (Model of Anticipation of flows and INondations for extreme Events) (Roux et al., 2011) is a dis-
tributed, physically based hydrological model. MARINE is tested by operational French flood forecasting services for flood
65 risk assessment. The recent developments of the MARINE model proposed by Douinot et al. (2018) lead to an improved rep-
resentation of the subsurface flow. These developments enhance the degree of refinement of the soil physics described in the
model. The impacts of this representation of the subsurface on the water discharge are extensively studied by Douinot (2016).
However, their influence on the spatial dynamic of soil saturation has not yet been explored.

70 Thus this work aims to assess the impacts of the developments proposed by Douinot et al. (2018) to include a physically ori-
ented soil representation in MARINE, with respect to the soil saturation dynamics during flash flood events. The performances
of the model are estimated with respect to several soil moisture products: i) The gridded soil moisture product provided by the
operational modeling chain SAFRAN-ISBA-MODCOU, available at the 8 km x 8 km spatial resolution ; ii) The gridded soil
moisture product provided by the LDAS-Monde assimilation chain, based on the ISBA-a-gs land surface model and assimi-
75 lating high resolution spatial remote sensing data. This work uses the version of LDAS-Monde at the 2.5 km x 2.5 km spatial
resolution ; iii) the upper soil moisture hourly measurements taken from the SMOSMANIA observation network; iv) The Soil
Water Index provided by the Copernicus Global Land Service (CGLS), available at the kilometric resolution and derived from
Sentinel1/C-band SAR and ASCAT satellite data. The comparison between the MARINE output for soil saturation dynamics
and these three sources of data is performed both at the local point measurement scale and at the catchment scale. These prod-
80 ucts represent valuable indicators of the spatio-temporal dynamics of soil moisture at various scales.

In section 2, the MARINE model along with its new developments for the soil model are described, together with the two
catchments and the events put under light for this study. The soil moisture products used in this work are also presented in this
section. In section 3, the methods employed for model set up and calibration and the comparison protocol are presented. The
85 last section consists in the results presentation and the last part opens the discussion concerning the validation of the simulation
of the water content of the deep underground zone.



2 Model and data

2.1 The Marine flash-flood model

2.1.1 Base model (BM)

90 The MARINE model (Roux et al., 2011) is a distributed, physically based hydrological model. MARINE consists of three
main modules: first, precipitation is separated between surface runoff and infiltration using the Green and Ampt model; then
the subsurface flows are represented using an approximation of the Darcy's law; finally, the overland and river fluxes are
simulated using the Saint-Venant equations simplified with kinematic wave approximation. Based on sensitivity analyses of
the model (Garambois, 2012), five parameters are calibrated in MARINE for the representation of the soil and the surface: the
95 multiplier coefficient for soil depth maps (C_z), the multiplier coefficient for the spatialized saturation hydraulic conductivity
used in lateral flow modelling ($C_{k_{ss}}$) the multiplier coefficient for the spatialized hydraulic conductivity at saturation that is
used in infiltration modelling ($C_{k_{ga}}$), and two friction coefficients for low and high-water channels.

2.1.2 The subsurface flow model (SSF)

This work uses the recent developments for the representation of the infiltration into the subsurface and the new two-layer
100 soil model proposed by Douinot et al. (2018). These new models are integrated into PLATHYNES, the modeling platform of
the French Service for Flood Forecasting (SCHAPI). In the MARINE base model, the transfers through the subsurface are
a function of the water height. However, Douinot et al. (2018) shows that expressing the subsurface flows as function of the
volumic soil water content of the cell instead of its water height appears to be a more appropriate choice to represent the
activation of preferential paths. Thus, Douinot et al. (2018) define a new subsurface flow model (SSF) where the lateral flows
105 are expressed as a function of the volumic soil water content of the cell.

2.1.3 The two soil layers model (SSF-DWF)

In the soil model initially implemented in MARINE (base model, see section 2.1.1), the soil is represented by a single layer.
Douinot et al. (2018) proposes a version of the soil model for which two soil layers are defined: the deep water flow model
(DWF). With the DWF soil model, the soil column is subdivided by two layers which represent the 'upper soil' part and the
110 'weathered rock' part of the soil. This subdivision involves the definition of two new flows, in addition to the lateral flow in
the upper soil to represent 1) the flows between the cells and the flows towards the drainage network in the weathered rock and
2) the vertical infiltration flow, from the 'upper soil' layer to the 'weathered rock' layer. In this DWF model, the depth of the
upper layer is equal to the soil depth provided by the soil data base and the deep layer has an uniform depth over the catchment.
The deep layer depth is calibrated for each catchment.

115

The two hypotheses made for the SSF and the DWF models can be merged to create the SSF-DWF model for the subsurface
flow representation in MARINE: in the SSF-DWF model, the soil column is separated into two layers. Vertical and lateral



transfers in the upper soil layer are described as a function of volumic soil moisture. In the SSF-DWF, the flows in the deep layer remains a function of the water height. The integration of the SSF-DWF model in MARINE necessarily implies the calibration of two additional parameters: 1) the ratio between of the hydraulic conductivity at saturation for the upper soil layer and for the deep layer; 2) the uniform depth of the deep layer. Extensive descriptions of the DWF, the SSF and the SSF-DWF model's physics and parametrization are presented in Douinot et al. (2018). The above-named acronyms are consistent with the ones used by Douinot et al. (2018).

2.2 Studied cases

2.2.1 The Ardeche at Vogue and the Orbieu at Lagrasse catchments

In this work, the study case is performed over two catchments located in the South of France, particularly submitted to flash flood events: the Ardeche river at Vogue and the Orbieu river at Lagrasse. These two catchments have been selected for this study because i) numerous flash flood events have been inventoried over the last decade over these catchments (Gaume et al., 2009) and ii) one SMOSMANIA station (Calvet et al., 2007) is installed since 2006 within each of these catchments for real-time superficial soil moisture measurements (see section 2.3.4).

Figure 1 presents the geographic situation of these two catchments. The digital elevation model (DEM) from the French Geographic Institute (IGN) at the 25-m resolution is considered in this work. The pedological information is taken from the French national institute for agronomic research (INRA) soil data base for the Ardeche and Languedoc-Roussillon regions. The land cover information is taken from the Corine Land Cover 2006 data base (Aune-Lundberg and Strand, 2010).

The Ardeche catchment (622 km^2 , from 193 m.a.s.l. to 1347 m.a.s.l.) is located in the Cevennes region, exposed to intense precipitation events due to the convection of humid sea air masses over the Cevennes mountain slopes. The Orbieu catchment (236 km^2 , from 135 m.a.s.l. to 807 m.a.s.l.) is also exposed to Mediterranean extreme events, in particular with the dramatic flood event of October 2018. The Ardeche catchment presents a mixed geology, globally with metamorphic rocks and schists on the upper part of the catchment and sedimentary plains downstream (source: www.infoterre.brgm.fr). The land cover for the Ardeche catchment is mainly mixed forest, natural grasslands and shrubs. The Orbieu catchment consist in a sedimentary area, mainly covered by arable land. Both catchments are little anthropized. The soil is 27 cm deep on average for the Ardeche catchment, with depths between 5 cm and 50 cm, and 37 cm deep on average for the Orbieu catchment, with depths between shallow and 73 cm. The soil texture is mainly sandy-loam for the Ardeche catchment, with silt deposits downstream and it is mainly silt and silty-loam for the Orbieu catchment. Extensive geomorphological descriptions of these two catchments can be found in Adamovic et al. (2016); Douinot (2016) and Garambois et al. (2016).

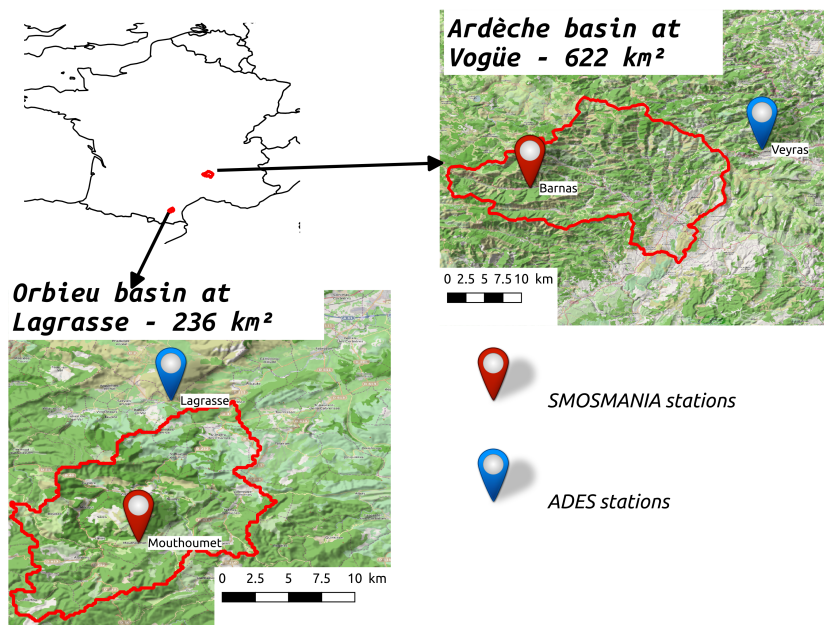


Figure 1. The two studied catchments located in the South of France: the Ardeche river at Vogue and the Orbieu river at Lagrasse. Monitoring networks: soil moisture (SMOSMANIA network stations) and the national groundwater ADES network stations (www.ades.eaufrance.fr).

2.2.2 The studied events

In this work, the ANTILOPE quantitative precipitation estimates (QPE) (Champeaux et al., 2009) are used for precipitation estimation. The ANTILOPE-QPE are based on a fusion between the radar data provided by the operational radar network ARAMIS (Tabary, 2007) and the measurements at pluviometers, spatialised by krigging method. ANTILOPE-QPE precipitation are available on the hourly time step, at the kilometric resolution. The criticized observed discharges at the outlet of the two catchments are taken from the hydrometric French database (www.hydro.eaufrance.fr). Table 1 presents the characteristics of the studied event.

155

Three flash flood events are considered for each catchments over the 2017-2019 period. The heterogeneity of the studied events has to be noted: for the Orbieu catchment, the extreme event of October 2018 represents the historical maximum for this region, with well known dramatic damages to infrastructures and populations. This flood has the particularity to be extremely fast, with about two hours between the precipitation peak and the discharge peak at the Lagrasse station. This response time appears to be faster than the response time regularly considered for this station (about 5 hours). On the opposite, the two other events considered for the Orbieu catchment, in February and Mars 2017, represent relatively small floods, with return periods of five years and two years, respectively. For the Ardeche catchment, the 2018 autumn has the particularity to present a serie of intermediate flood events. For this period, the damages have mainly been induced by the duration of the flooding period.

160



For the event defined for this study (November 2018, 22nd to 28th), the precipitation amounts do not represent extreme value, however, flood damages have been noticed during this period. In addition, different hydrological responses can be distinguished for spring or autumn seasons, due to different soil and vegetation conditions, possible snow contribution and meteorological antecedents. This variety in the structures of the six events considered for this study represents both a robustness guaranty and a challenge for the modeling exercise.

Table 1. The six events considered in this work for the Ardeche at Vogue and the Orbieu at Lagrasse catchments, with cumulated volume (Precip.) and maximal intensity (I_{max}^{pr}) of ANTILOPE-QPE precipitation, maximal hourly observed discharge (Q_{max}^{obs}). The stars indicate the return period of the flood: (*) for a 2-years, (**) for a 5-years, and (***) for a 100-years return period. The given dates and duration are the ones considered for the hydrological simulations. S.M. is the initial soil moisture provided by the SAFRAN-ISBA-MODCOU chain for the first day of the simulations, on average over the catchment.

Event	Ardeche catchment			Orbieu catchment		
	Ev 03 2018*	Ev 11 2018**	Ev 04 2019*	Ev 02 2017**	Ev 03 2017*	Ev 10 2018***
Dates	09-20/03	22-28/11	23-29/04	10-18/02	23-28/03	14-19/10
Duration	11days	6days	6days	8days	6days	4days
Precip.	170 mm	98 mm	146 mm	79 mm	58 mm	193 mm
I_{max}^{pr}	11 $mm.h^{-1}$	9 $mm.h^{-1}$	12 $mm.h^{-1}$	5 $mm.h^{-1}$	7 $mm.h^{-1}$	24 $mm.h^{-1}$
Q_{max}^{obs}	580 $m^3.s^{-1}$	627 $m^3.s^{-1}$	513 $m^3.s^{-1}$	181 $m^3.s^{-1}$	99 $m^3.s^{-1}$	448 $m^3.s^{-1}$
S.M.	57.62 %	62.69 %	50.81 %	55.5 %	53.8 %	47.83 %

2.3 Soil moisture products available

2.3.1 The SAFRAN-ISBA-MODCOU products

The SAFRAN-ISBA-MODCOU operational modeling chain (SIM) (Habets et al., 2008) uses the ISBA surface scheme, coupled with the MODCOU hydrological model for underground flows and forced by the SAFRAN atmospheric reanalysis. SIM outputs are available since 1958, on an hourly basis, on a regular mesh at the 8-km resolution. In particular, SIM provides moisture data for the root layer of the soil. This work uses the outputs of two available versions of SIM: 1) SIM1, which uses the force-restore version of ISBA, ISBA-3L (Noilhan and Planton, 1989; Noilhan and Mahfouf, 1996); and 2) SIM2, which uses the diffusive version of ISBA, ISBA-DIF (Decharme et al., 2011), with a vertical soil column discretization into a maximum of 14 layers. In ISBA-3L, the root zone moisture corresponds to the humidity of the second soil layer. In ISBA-DIF, the humidity of the root zone is considered as the sum of the humidities of the ISBA-DIF layers between 10 cm and 30 cm deep for this specific study. The daily soil humidities of SIM correspond to the value at 06 UTC each day. In this work, the root zone moisture provided by the SIM1 product is used for the initialization of the soil saturation in MARINE, as it is the product used by Douinot (2016) and Garambois (2012) to calibrate the MARINE model. The SIM2 soil moisture data is compared to the MARINE soil moisture outputs.



2.3.2 The LDAS-Monde product

LDAS-Monde (Albergel et al., 2017) assimilates satellite derived data into the ISBA land surface model. It uses the ISBA-
185 A-gs (Calvet et al., 1998) model, the CO_2 -responsive version of ISBA. The diffusive version of ISBA (ISBA-DIF) is used.
ISBA-A-gs allows to simulate photosynthesis and fluxes of CO_2 . In addition, LDAS-Monde assimilates LAI (Leaf Index Area)
data provided by the European service Copernicus Global Land (CGLS), with a sequential assimilation algorithm (Simplified
Extended Kalman Filter). The contribution of the assimilation of satellite data for the simulation of surface fluxes has been
tested for various application cases, in particular over Europe and France by Fairbairn et al. (2017), Leroux et al. (2018),
190 Dewaele et al. (2017) and Barbu et al. (2011). In this work, the version of LDAS-Monde which uses the AROME atmospheric
model outputs for the atmospheric forcing of the model is used (Albergel et al., 2018; Bonan et al., 2020). These AROME-
forced outputs are available since July 2017, at the 2.5 kilometer resolution and at three-hour time steps.

2.3.3 Satellite derived products

Various products derived from remote imagery are available for soil moisture estimation, at various spatial and temporal scales.
195 In particular, the relevance of five products is investigated for this study. Table 2 summarizes the investigated products and their
main characteristics.

Table 2. Investigated satellite derived soil moisture products and their main characteristics: data produced, provided variable, spatial resolution, satellite imagery employed and associated average uncertainties when provided. NA stands for Not Applicable.

Shortname	Producer	Variable	Spatial resol.	Satellite source	Uncertainty	Reference
CGLS SWI	CGLS	SWI	1 km	Sentinel-1, MetOp/ASCAT	NA	(Bauer-Marschallinger et al., 2018a)
CGLS SSM	CGLS	SSM	1 km	Sentinel-1	8%	(Bauer-Marschallinger et al., 2018a)
THEIA VHSR	THEIA-Land	SSM	1 km	Sentinel-1, Sentinel-2	NA	El Hajj et al. (2017)
SMOS-IC	INRA-CESBIO	SSM	25 km	SMOS L3	5%	Fernandez-Moran et al. (2017)
ESA CCI	ESA	SSM	25 km	AMI-WS, MetOp/ASCAT	3%	Dorigo et al. (2015, 2017)

- The Copernicus Global Land Service (CGLS) provides both Surface Soil Moisture (SSM) and Soil Water Index (SWI) values at the 1-km spatial resolution and at the daily time step (Bauer-Marschallinger et al., 2018a). The SWI product combines the Sentinel-1/C-SAR band data and the MetOp/ASCAT data, in accordance with the algorithm presented by Bauer-Marschallinger et al. (2018b), whereas the SSM product is derived from only the Sentinel-1/C-SAR band data. In this work, the SWI values provided for the top 5 cm soil are considered. The uncertainties for the CGLS SSM are computed by adding the different sources of uncertainty occurring in the product preparation and they represent about 8% of the SSM values. No uncertainties estimation is provided for the SWI product.



- 205
- The soil moisture with very high spatial resolution product (VHSR) (El Hajj et al., 2017), provided by the THEIA-Land pole (www.theia-land.fr), offers soil moisture maps with a 6-days frequency and at the sub-parcel scale on several sites in France, in Europe and around the Mediterranean basin. The THEIA-Land VHSR soil moisture product exploits the Sentinel-1 radar and Sentinel-2 optical Copernicus image series, following a neural networks signal inversion algorithm. The extent of the two studied basins is globally covered by this product. However, the footprints of the images being

210

variable depending on the dates, the whole catchments are not covered for all dates. The amount of gaps in this product is significant: only 12 images are available over the studied events. In particular, no data are available over the Ardeche catchment for the studied dates.

 - The SMOS-IC product (Fernandez-Moran et al., 2017) provides daily SSM at the 25-km resolution. The SMOS-IC soil moisture are derived from the SMOS remote data, based on the algorithm presented by Wigneron et al. (2007). This

215

method uses the new calibrated values of the soil roughness and effective scattering albedo parameters presented by Li et al. (2020). The uncertainties associated with the SMOS-IC product are estimated through the TB-RMSE index, presented by Al-Yaari et al. (2019) and represent about 5% of the SMOS-IC SSM values.

 - The ESA CCI product provides surface soil moisture datasets at daily temporal time step and 25 km spatial resolution. In this product, the AMI-WS and MetOp/ASCAT/C-band data are merged with several radiometer soil moisture products,

220

along the algorithm presented by Wagner et al. (2012). The uncertainties associated with the ESA CCI SSM product is considered as the variance of the dataset, estimated through triple collocation analysis. Uncertainties represent about 3% of the ESA CCI SSM values.

Figure 2 jointly displays the catchment average for these products over the studied events, as well as their respective fraction of missing values. The impact of the spatial resolution on the spatially averaged values can be clearly noticed. The coarse

225

resolution (e.g. 25 km and 30 km resolution) SMOS-IC and ESA CCI soil moisture products appear to be overall lower than the products at the kilometric resolution (CGLS and THEIA-Land VHSR). In addition, the ESA CCI product is known to provide globally wetter SSM than the SMOS-IC product, as mentioned by Dong et al. (2020). However, it is to be noted that this products inter-comparison is mainly informative regarding the products temporal dynamics but their respective biases cannot be directly compared, mainly for two reasons: i) the compared variables are not necessarily commensurable (i.e. SSM

230

and SWI); ii) the soil depth considered in each product for the SSM estimation might differ.

Important discrepancies are observed in the temporal dynamics for the different product. Since the study area is rather small, no validation of these products at the very local scale is available and the relatively low uncertainties estimates do not allow to explain these differences (see table 2). As no particular temporal behavior can be distinguished among the five product, the

235

choice has been done for this work to particularly focus on the product that offered the most important data availability and the finest spatial resolution. The amounts of missing values for the SMOS-IC and the THEIA-Land VHSR products, and also for the CGLS SSM products are too important for these data sources to be reliably used. On the contrary, the CGLS SWI product presents a good data availability, despite some events being less covered than others (e.g. March 2018 or November



2018 over the Orbieu catchment). In this product, the number of informative pixels per catchment for the studied cases is greater than 14% of the catchment area. Consequently, in this work, the CGLS SWI product is taken into account to perform the comparison with the soil moisture simulated in MARINE. Nevertheless, this literature exploration of the data available for soil moisture description illustrates the difficulty to estimate surface soil moisture based on satellite data at small catchment scale ($\sim 100\text{km}^2$).

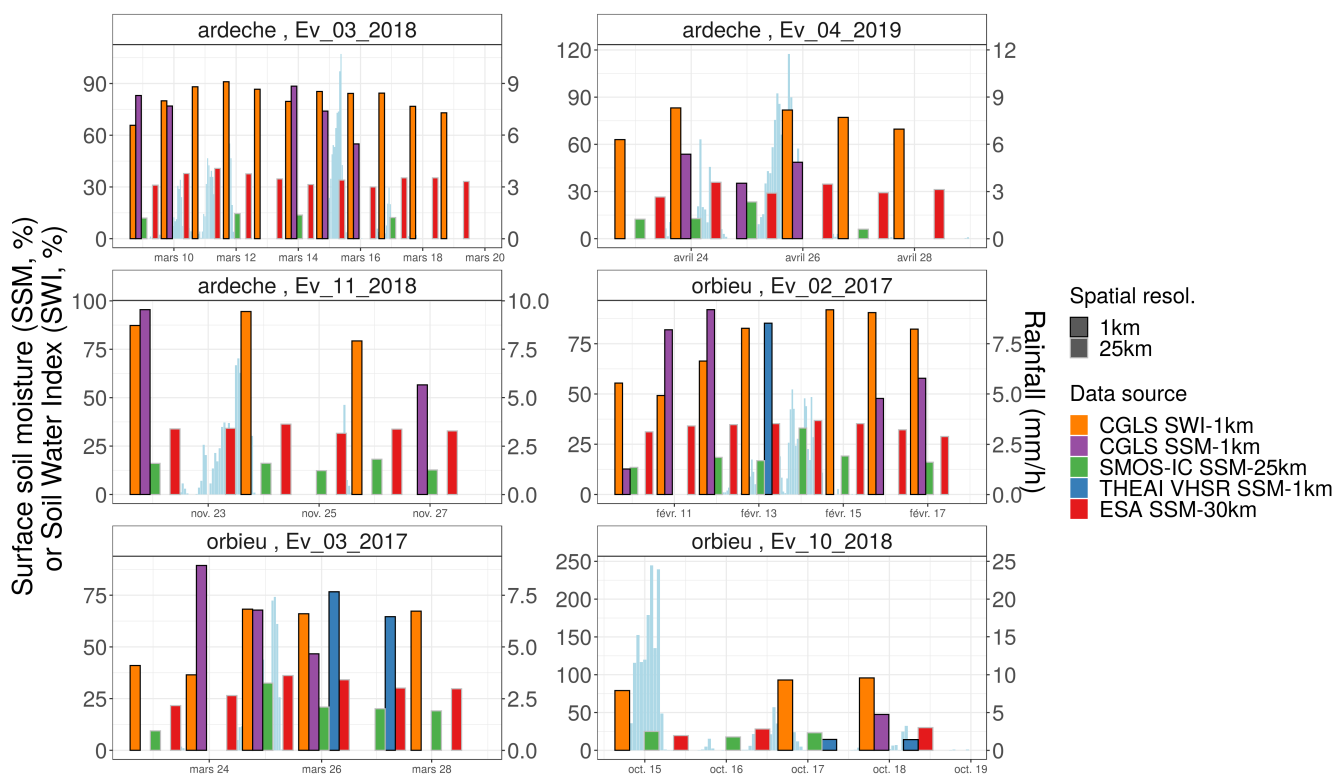


Figure 2. Daily values of Surface Soil Moisture (SSM) or Soil Water Index (SWI) provided by the CGLS, SMOS-IC, THEIA-Land VHRS and ESA CCI products (left axis), along with associated ANTILOPE precipitation (right axis), on average over the two studied catchments during the six simulated events.

2.3.4 The SMOSMANIA network

245 The SMOSMANIA project (Soil Moisture Observing System Meteorological Automatic Network Integrated Application, Calvet et al. (2007); Parrens et al. (2012)) provides soil moisture measurements for 21 stations of the automatic ground station network of Météo-France (the RADOME network), along a 400 km Mediterranean-Atlantic transect in southwestern France. Each SMOSMANIA station is equipped with four ThetaProbes ML2X instruments forming a soil profile at the depths 5, 10, 20, 30 cm. Volumetric soil moisture is recorded at each depth and data are transmitted each 15 minutes since 2006 for all



250 the stations. Two stations are considered for this work: the Mouthoumet station, located inside the Orbieu at Lagrasse catchment, and the Barnas station, located inside the Ardeche at Vogue catchment. For these two stations, soil moisture profiles are available over the whole 2017-2019 period. The sensors calibrations are regularly checked and the vertical variability of soil properties is taken into account for these calibrations.

2.3.5 The ADES piezometric network

255 The ADES database (Access to Data on Groundwater, www.ades.eaufrance.fr), coordinated by the French National Geological Survey (BRGM), provides piezometric level measurements throughout France. One point of measurement is available for each of the two studied catchment. Figure 1 shows the location of the two measurement points. For the Orbieu catchment, the water table is 110 km^2 large and 1849 km^2 large for the Ardeche catchment. The measurements are available at the daily time step and the daily value represents the maximum of the water level measurements in 24 hours. In this work, the relative underground
260 water level with respect to the measurement mark is compared to the water content of the deep layer simulated with SSF-DWF model.

3 Methods

3.1 Comparison protocol

3.1.1 Choice of layers for the LDAS-Monde soil moisture

265 Figure 3 presents the spatial average of the soil moisture, for each catchment and for each of the eleven soil layers described in the LDAS-Monde product. Two behaviors can be distinguished for the different layers: for the five superficial layers, a fast-responding soil moisture and a more stable soil moisture, with a slower response to precipitation and narrower amplitude range for the deeper layers. Moreover, the diurnal cycle of solar radiation significantly influences up to the fifth layer, i.e. up to 40 cm deep. In addition, over the two studied catchments, the spatial patterns of soil moisture are similar for the eleven
270 layers. Indeed, the spatial distribution of soil moisture is mainly controlled by the soil texture, which is considered as vertically uniform in the ISBA-A-gs model. Consequently, the choice is made in this work to synthesize the eleven LDAS-Monde layers as three average layers: the surface layer (average of layers 1 to 5), the deep layer (average of layers 6 to 11), and the total layer (average of all the 11 layers). Thus, the surface layer represents depths from 0 cm to 40 cm and the deep layer represents depths from 40 cm to 300 cm. Concerning the comparison between the MARINE simulation and LDAS-Monde, for the base and SSF
275 models, which use a one layer soil discretization, the MARINE soil moisture is compared to the moisture of the surface layer, noted HU_{surf} . For the SSF-DWF model, which uses a two-layers soil discretization, the moisture of the MARINE upper layer is compared to LDAS-Monde surface layer, and the moisture of the MARINE deep layer is compared to the LDAS-Monde deep layer (noted HU_{deep}). The total average LDAS-Monde layer is used for overall comparison.

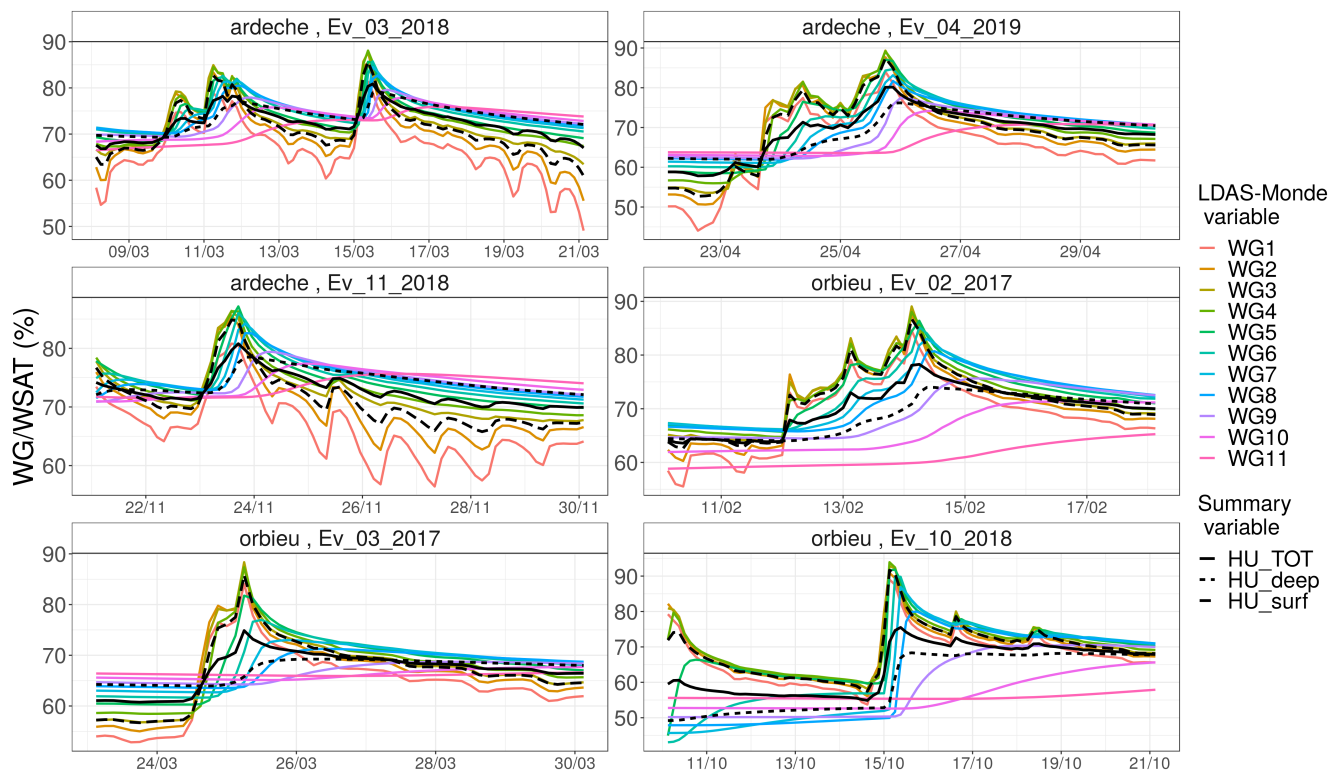


Figure 3. Soil moisture (%) for the 11 soil layers described in LDAS-Monde and summary variables HU_{surf} (average of the layers 1 to 5), HU_{deep} (average of the layers 6 to 11) and HU_{tot} (average of the layers 1 to 11), in average per catchment for the six studied events.

3.1.2 Method for comparing gridded data to SMOSMANIA observations

280 The SMOSMANIA observation network provides valuable information for the upper soil water content. However, it raises the issue to compare point measurements to the gridded simulated soil moisture. Various strategies might be used to face this issue, among which averaging at a large time scale (Tramblay et al., 2010; Fuamba et al., 2019). In this study, considering the fast-evolving processes involved, we choose to maintain the hourly time step for soil moisture analysis. The important spatial variability of the soil moisture is then taken into account by spatial averaging the gridded simulated values around the measurement point.

285 In order to consider equivalent surfaces for the grids simulated in MARINE and provided by the LDAS-Monde and CGLS data, the MARINE soil moisture maps are averaged on a 1 km^2 area around the measurement point. In addition, the MARINE drainage network is excluded from this average area, because the physics of the soil saturation in the drainage network is not commensurable with its physics over hillslope meshes. This leads to exclude 4 meshes over 16 from the average area for the Ardeche catchment, and no mesh for the Orbieu catchment.



290 3.1.3 Indices

The performance of the simulated discharges are estimated at the hourly time step through the usual Nash Sutcliffe Efficiency criteria (NSE) and also through the LNP index, defined by Roux et al. (2011) as in equation 1, where Q^{obs} (Q_{max}^{obs}) and Q^{sim} (Q_{max}^{sim}) represent the (maximal) observed and simulated discharged, respectively, and $T_{concentration}$, the concentration time of the catchment. The advantage of the LNP index is to give equal weight to the NSE values (first term), to the peak value estimation (second term) and to the timing of the peak simulation (third term). LNP appear to be a integrative criteria well-suited for flash flood modelling (Lovat et al., 2019).

$$LNP = \frac{1}{3} \cdot \left(1 - \frac{\sum_i (Q_i^{sim} - Q_i^{obs})^2}{\sum_i (Q_i^{obs} - \overline{Q_i^{obs}})^2}\right) + \frac{1}{3} \cdot \left(1 - \frac{|Q_{max}^{sim} - Q_{max}^{obs}|}{Q_{max}^{obs}}\right) + \frac{1}{3} \cdot \left(1 - \frac{|T_{max}^{sim} - T_{max}^{obs}|}{T_{concentration}^{obs}}\right) \quad (1)$$

The comparison of the soil moisture simulated in MARINE and provided by LDAS-Monde is performed at the catchment scale using the relative bias and the Kendall correlation over values averaged at the catchment scale. In addition, the spatial dynamics of the simulated soil moisture are quantified using the spatial moments δ_1 and δ_2 defined by Zoccatelli et al. (2011). The δ_1 and δ_2 moments take into account the distance of each grid cell to the drainage network and they allow to represent both the overall location of the soil moisture field with respect to the outlet and the number of modes (i.e concentration points in this case) of the field. The closer of 1 are the δ_1 values, the more centred around the centroid of the catchment is the field. Values of δ_1 lower that 1 mean that the field get closer from the outlet, whereas values higher that 1 characterize a field overally located on the highest areas of the catchment. The closer of 1 are the δ_2 values, the more uniform is the distribution of the field. Values of δ_2 lower that 1 represent an unimodal distribution and values of δ_2 higher that 1 mode likely represent a multimodal distribution. Despite being initially defined by Zoccatelli et al. (2011) to characterize rainfall fields, the δ_1 and δ_2 moments also appear to be particularly relevant when applied to soil moisture fields.

310 3.2 Model set up

3.2.1 Parametrization and precipitation forcing

The MARINE model requires the definition of i) the digital elevation model (DEM), ii) soil survey data to compute the hydraulic and storage properties of the soil and iii) land-use data to configure the surface roughness parameters. The IGN-25 m DEM is used in this work. The soil depths and soil texture maps are taken from the INRA soil data base for the Ardèche and Languedoc-Roussillon regions (Robbez-Masson et al., 2000). The parameters of the pedotransfer function are computed based on the USDA soil classification (Spaargaren, 1995). Land cover is provided by the Corine Land Cover 2006 data base (Aune-Lundberg and Strand, 2010). The model is set up over a regular mesh, with a 200 m spatial resolution for the Orbieu catchment and a 250 m resolution for the Ardeche catchment. The model computation time step is 5 minutes and results are aggregated at the hourly time step. This study uses the calibration of MARINE provided by Garambois et al. (2015) for the Orbieu catchment



320 and by Douinot (2016) for the Ardeche catchment. The ANTILOPE QPE data are used as hourly precipitation input for the MARINE model, available at the kilometeric resolution. Figure 4 presents the IGN-25 m DEM and the soil depth maps used for the two studied catchments. Table 3 presents the calibrated parameter values obtained for each catchment by Douinot (2016) and Garambois et al. (2015) and used in this work.

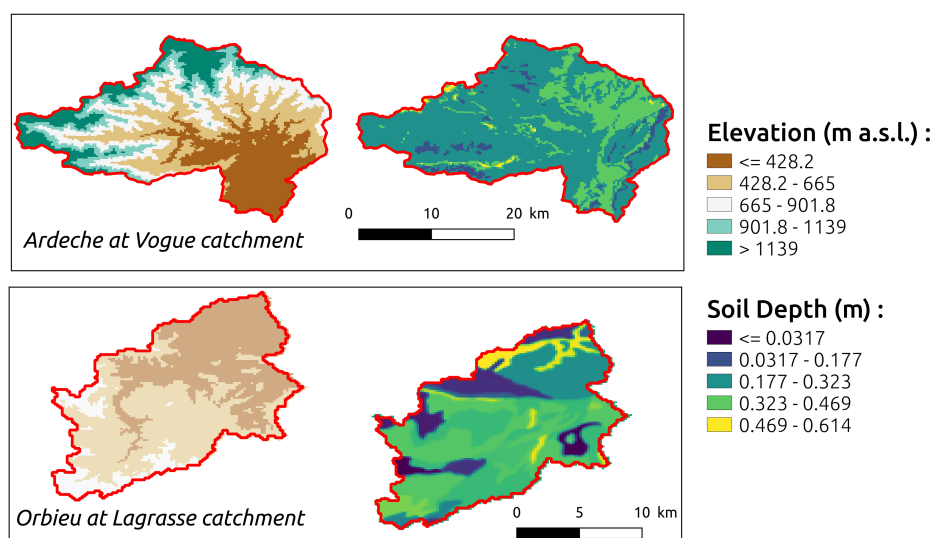


Figure 4. The IGN-25 m DEM and soil depth maps from the INRA soil data base used for MARINE parametrization for the two studied catchments.

Table 3. Calibrations obtained by Douinot (2016) and Garambois et al. (2015) for the Orbieu at Lagrasse and Ardeche at Vogue catchments: the multiplier coefficient for soil depth maps (C_z), the multiplier coefficient for the spatialized saturation hydraulic conductivity used in lateral flow modelling (C_{kss}) the multiplier coefficient for the spatialized hydraulic conductivity at saturation that is used in infiltration modelling (C_{kga}), two friction coefficients for low and high-water channels (C_{D1} and C_{D2}), and deep layer depth for the SSF-DWF model (C_z^{deep}).

Basin:		Ardeche	Orbieu
Calibration:		Douinot (2016)	Garambois et al. (2015)
C_z	(-)	2.86	1.3
C_{kga}	(-)	1.34	15
C_{kss}	(-)	3241	10000
C_{D1}	($m^{1/3}.s^{-1}$)	14.4	9.1
C_{D2}	($m^{1/3}.s^{-1}$)	18.5	2
C_z^{deep}	m	1.42	0.51



3.2.2 Discharge simulation

325 Figure 5 presents the discharges at the outlets, simulated with MARINE using the base, the SSF or the SSF-DWF models together with the observed discharges during the flood events. Table 4 presents the associated LNP and Nash Sutcliffe Efficiency (NSE) performance criterias of the simulated discharges, referring to hourly observed discharges. The main effect of computing the transfers through the subsurface as a function of the volumetric soil water content instead of the water height (SSF model) is to flatten the overestimation of the simulated discharge during the flow rise, at the beginning of the events. This behavior will be explained in the result section: there is no gradient of initial soil water content over the 8x8km SIM mesh and therefore smaller subsurface contribution at the beginning of the events in the SSF and SSF-DWF. However, in the SSF-DWF model, this dynamics is influenced by the contribution of the deep layer, itself mainly controlled by the parametrization of the thickness of this deep layer. Nevertheless, the calibrations of the three models clearly require to be improved in order to better simulate the discharges at the outlets, in particular for the Orbieu catchment and for the SSF-DWF model. However, since this paper focuses on comparing the soil moisture dynamic simulation according to the soil physics considered in the model, and considering that the variety in the structures of the considered events (see section 1) is a limit to model performances, the calibration proposed by Douinot (2016) and Garambois et al. (2015) are directly applied to this work.

Table 4. LNP and Nash Sutcliffe Efficiency (NSE) performance criterias for discharges simulation at the outlet for the six studied events over the two catchments, for the base, the SSF and the SSF-DWF models, referring to hourly observed discharges.

Ardeche catchment				Orbieu catchment			
Event	Model	LNP	NSE	Event	Model	LNP	NSE
Ev 03 2018	BM	0.79	0.57	Ev 02 2017	BM	-0.36	-2.46
Ev 03 2018	SSF	0.63	0.24	Ev 02 2017	SSF	0.26	0.38
Ev 03 2018	SSF-DWF	0.49	0.09	Ev 02 2017	SSF-DWF	-0.09	-1.28
Ev 04 2019	BM	0.58	-0.12	Ev 03 2017	BM	-3.55	-11.27
Ev 04 2019	SSF	0.26	0.75	Ev 03 2017	SSF	0.25	0.23
Ev 04 2019	SSF-DWF	0.15	0.69	Ev 03 2017	SSF-DWF	-1.62	-5.93
Ev 11 2018	BM	0.76	0.44	Ev 10 2018	BM	-0.43	-2.28
Ev 11 2018	SSF	0.57	0.15	Ev 10 2018	SSF	0.26	-0.31
Ev 11 2018	SSF-DWF	0.73	-0.37	Ev 10 2018	SSF-DWF	-0.19	-1.56

4 Results and discussions

4.1 Comparison at the point measurement scale

340 Figure 6 puts together i) the soil moisture measurement at the four sensor depths for the Barnas (for the Ardeche catchment) and the Mouthoumet (for the Orbieu catchment) SMOSMANIA stations; ii) the soil moisture simulated with MARINE, on

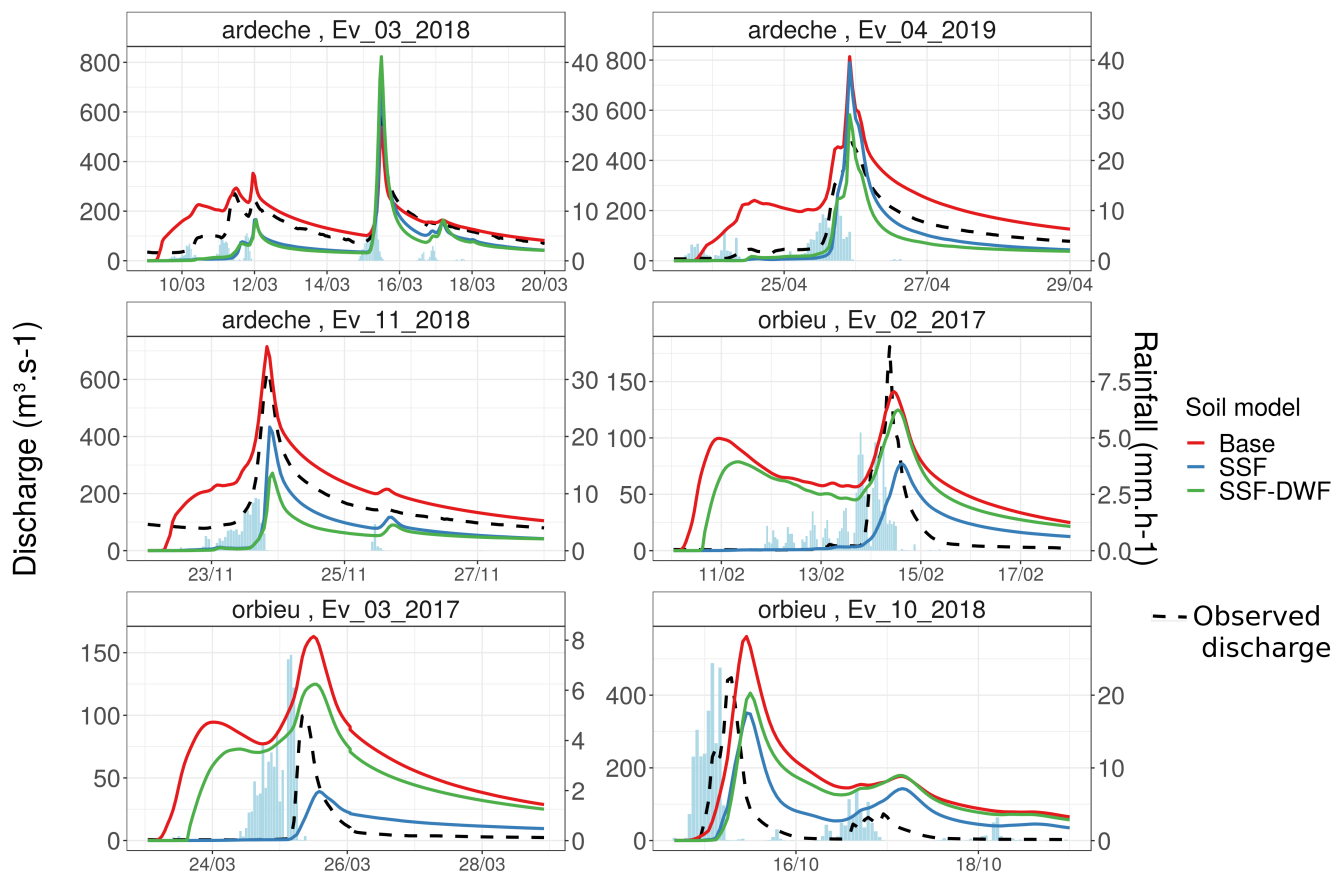


Figure 5. Discharges at the outlets, simulated with MARINE using the base, the SSF and the SSF-DWF models, and observed discharges.

average over a 1-km^2 area over the station location (see section 3.1.2). For the simulations using the SSF-DWF soil model, the moisture of the surface layer is considered here; iii) the LDAS-Monde surface soil moisture HU_{surf} for the $2.5\text{ km} \times 2.5\text{ km}$ grid cell that contains the SMOSMANIA station; iv) the CGLS SWI when available for the $1\text{ km} \times 1\text{ km}$ grid cell that contains the SMOSMANIA station for the Orbieu catchment. No data are available for the grid cell that contains the station for the Ardeche catchment. Table 5 provides the Kendall correlations associated with the hourly time series presented on figure 6. The values in bold are the best correlation values between the SMOSMANIA measurements and the MARINE outputs or the LDAS-MONDE HU_{surf} for each event.

Soil moisture simulated with the base model significantly differs from the simulations using the SSF and the SSF-DWF models: the soil layer empties faster with the base model, leading to a simulated soil moisture significantly lower with the base model than with the two other models. Overallly for the simulated events, the simulated soil moisture and the SMOSMANIA measurements appears to be better correlated when using the SSF-DWF model rather than the base model or the SSF model.



The soil physics used in the SSF-DWF, i.e. the use of the volumic soil water content rate and the vertical discretization into two
355 layers, allows to enhance the soil moisture simulation for the surface layer, with respect to in-situ measurements. This point
will be developed by considering the catchment average of simulated soil moisture in the next section.

In addition, the soil moisture simulated for the surface layer with the SSF-DWF is globally higher than for the two other
models. This behavior can be explained by the fact that, for the SSF-DWF model, soil depths are taken from the INRA soil data
360 base, whereas for the base model and SSF model, a multiplicative, calibrated coefficient superior to 1 is applied. Consequently,
the depths considered for the surface layer are thinner in the SSF-DWF than in the base model and SSF model. The saturation
of the surface layer is then reached faster.

Besides, the LDAS-Monde HU_{surf} appears to be globally satisfyingly correlated with the SMOSMANIA measurements,
365 with slightly different correlations for the four sensor depths. This shows that the dynamic of the LDAS-Monde HU_{surf}
variable is locally significant with in-situ surface soil moisture measurement. The reliability of the LDAS-Monde HU_{surf}
dynamic for surface soil moisture description can thus be considered as satisfying. On the contrary, the correlation between the
daily CGLS SWI values and both the MARINE outputs and the SMOSMANIA measurements appear to be low. However, a
more extensive study of the validity of this product at the local scale would be needed to draw further conclusions.

370 4.2 Comparison at the catchment scale

4.2.1 Water content of the surface layer

Figure 7 presents the soil moisture time series, on average per catchment, simulated with MARINE using the base, the SSF
or the SSF-DWF models, together with the catchment average of the LDAS-Monde HU_{surf} , the daily CGLS SWI values and
the daily SIM2 HU values (see section 2.3.1). When the SSF-DWF model is applied, the surface layer is considered here.
375 Table 6 presents the Kendall correlations associated with the hourly times series. The same observations as for the comparison
at the local scale can be drawn: both the dynamics and the amplitudes of the soil moisture simulated with the base model
significantly differ from the outputs of the two other models. When no precipitation happens, the soil drainage in the base
model is faster than for the SSF and the SSF-DWF models. In addition, the soil moisture simulated with the SSF-DWF model
is globally higher than the one simulated with the SSF model, on average per catchment. The soil moisture simulated with
380 the SSF-DWF model appears to be better correlated with the LDAS-Monde HU_{surf} time series, for four of the six studied
events. Considering that the dynamics of the LDAS-Monde HU_{surf} is of satisfying accuracy (see section 4.1), the SSF-DWF
model appear to improve the simulation of the dynamics of the surface layer moisture, compared to both the SSF and the
base models. This results appears to be particularly reliable, since it is observed both a the point measurement scale and at
the catchment scale. It can be physically explained by the fact that, in the SSF and the SFF-DWF models, the lateral transfers
385 are computed as a function of the volumic soil water gradients, whereas in the base model, they are computed as a function
of the water height gradient. Indeed, since the water height gradient between two cells depends on the slope between the cells

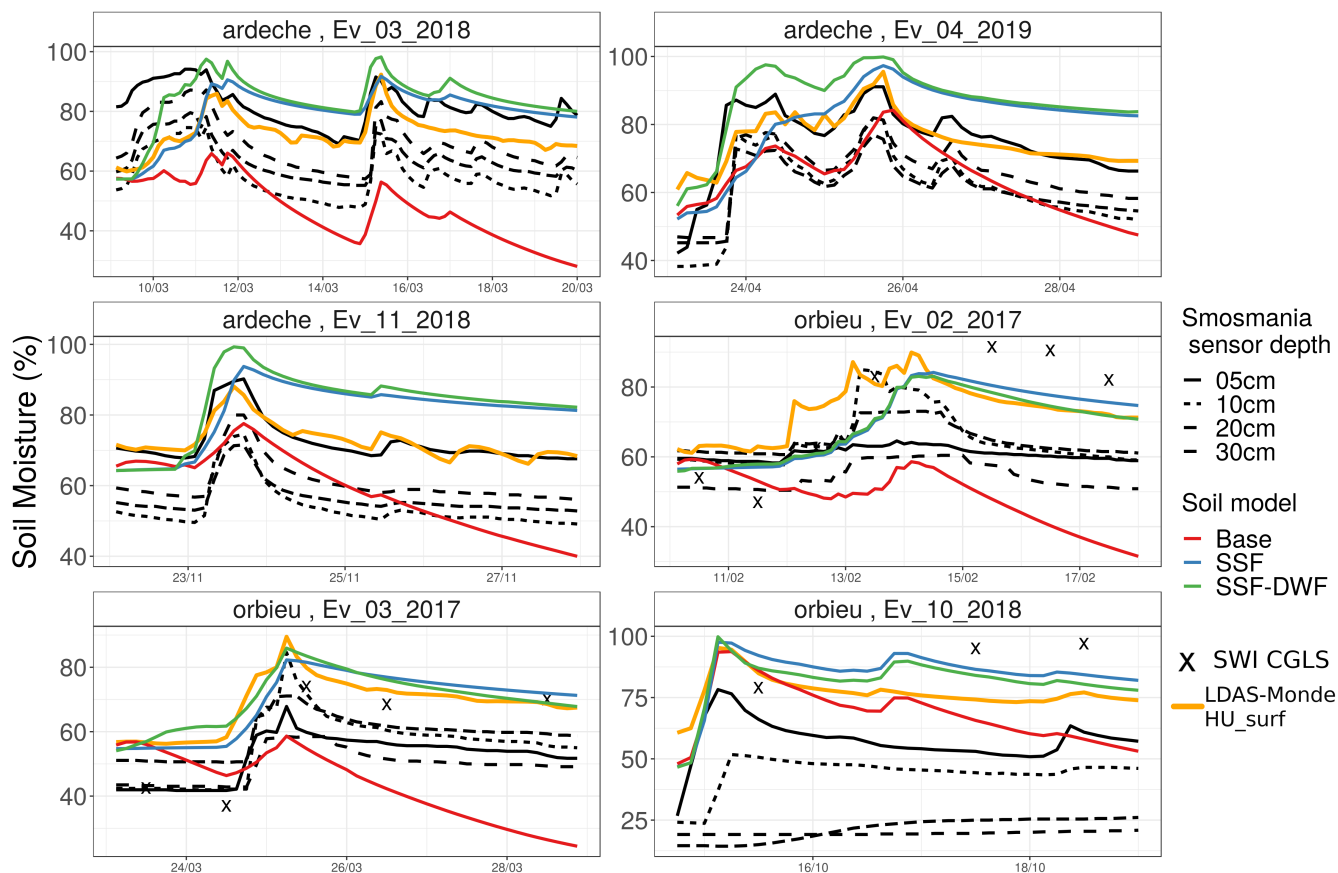


Figure 6. SMOSMANIA soil moisture measurement at the four sensor depths for the Barnas (Ardeche catchment) and the Mouthoumet (Orbieu catchment) stations, together with the soil moisture simulated with MARINE, the LDAS-Monde HU_{surf} and the CGLS SWI when available at the measurement point location. For the MARINE simulations using the SSF-DWF soil model, the moisture of the surface layer is considered here.

and the cells textures, water height gradients are larger than volumic soil water gradient when no precipitation happens. Consequently, lateral flows based on the water height gradients are larger than lateral flows based on the volumic soil water gradient.

390 On overall, the temporal dynamics of the CGLS SWI, in average per catchment is more consistent with the SSF and SSF-DWF models outputs than with the base model output. In particular, for the events of February and March 2017 on the Orbieu catchment, the sharp decreases of the soil moisture simulated in the base model is not observed in the CGLS SWI values. In addition, for the event of Novembre 2018 on the Ardeche catchment, which is the longest of the studied events, the dynamic of the CGLS SWI is very consistent with the soil moisture simulated with the SSF and SSF-DWF models. Likewise, catchment
 395 averages of the SIM2 HU values are also better correlated with the SSF and SSF-DWF models outputs than with the base



Table 5. Kendall correlations between Smosmania measurements at each depth and MARINE soil moisture simulated with each soil model or the LDAS-Monde HU_{surf} . The values in bold are the best correlations between the SMOSMANIA measurements and the MARINE outputs or the LDAS-MONDE HU_{surf} for each events.

Soil model	Depth	Orbieu catchment			Ardeche catchment		
		Ev 02 2017	Ev 03 2017	Ev 10 2018	Ev 11 2018	Ev 03 2018	Ev 04 2019
Base	05cm	0.254	0.239	0.512	0.569	0.452	0.69
Base	10cm	0.193	0.24	0.499	0.617	0.41	0.695
Base	20cm	0.248	0.261	-0.65	0.617	0.457	0.693
Base	30cm	0.207	0.211	-0.625	0.631	0.493	0.694
SSF	05cm	0.457	0.76	0.354	0.476	0.122	0.368
SSF	10cm	0.486	0.777	0.44	0.507	0.161	0.40
SSF	20cm	0.518	0.736	-0.435	0.571	0.19	0.416
SSF	30cm	0.569	0.744	-0.391	0.573	0.208	0.447
SSF-DWF	05cm	0.488	0.83	0.303	0.622	0.379	0.808
SSF-DWF	10cm	0.518	0.839	0.331	0.646	0.404	0.843
SSF-DWF	20cm	0.544	0.808	-0.4	0.698	0.427	0.855
SSF-DWF	30cm	0.59	0.801	-0.342	0.665	0.436	0.846
HU_{surf}	05cm	0.826	0.909	0.748	0.67	0.25	0.766
HU_{surf}	10cm	0.846	0.869	0.641	0.672	0.27	0.815
HU_{surf}	20cm	0.841	0.88	-0.537	0.649	0.285	0.814
HU_{surf}	30cm	0.779	0.819	-0.467	0.639	0.305	0.806

model output, despite the ranges of variation of the daily SIM2 HU values are narrower than the range for the CGLS SWI values.

Figure 8 presents maps of soil moisture simulated with the base, the SSF and the SSF-DWF models, and the maps of LDAS-Monde HU_{surf} , for the example of the event of November, 2018 on the Ardeche catchment. The daily products are not presented here because the daily time step does not allow to represent the fast-evolving flood processes. Four time steps of the simulation are considered: first time step of the run, one time step during the flow rise, the peak flow hour and one time step in the flow decreasing. This example illustrates the results previously described: the saturation of the surface layer is faster reached for the SSF-DWF model than in the others. In addition, the spatial pattern of the soil moisture simulated with MARINE appears to consistent with LDAS-Monde HU_{surf} maps. An other interesting result is that the soil moisture initialization pattern seems to be vanished after a few rainy simulation time step. These results are also observed for the other events, not presented here.



Figures 9 and 10 present the δ_1 and δ_2 spatial moments computed for the MARINE soil moisture outputs, for the LDAS-
 410 Monde HU_{surf} and for the CGLS SWI at the daily time step. Since no lateral transfers are represented in the LDAS-Monde
 and the CGLS SWI product, the MARINE drainage network is used to compute the spatial moments for both of them. The
 distinction between the base model outputs and the SSF and SSF-DWF model outputs can still be made. The general behavior
 of the δ_1 spatial moment when computed on the soil moisture is that the δ_1 increases when precipitation happens and then
 decreases at a variable rate. Indeed, precipitation that waters the catchment are doomed to flow toward the outlet. The δ_1 time
 415 series obtained with the base model appear to be significantly lower than for the SSF and the SSF-DWF models. This can be
 explained by the faster emptying of the upper soil layer in the base model than in the other two models. Indeed, faster lateral
 transfers from each cell to its downhill cell lead to soil moisture distribution overallly higher around the outlet at each time step.

The general behavior of the δ_2 spatial moment is that the δ_2 decreases with precipitation, with soil moisture fields more
 420 centered around the area of maximum rainfall, and then increases with the spread of the soil moisture fields along the drainage
 network. The δ_2 values for the SSF and SSF-DWF models are globally closer to 1 than for the base model. Indeed, since the
 soil saturation is globally higher for the SSF and SSF-DWF models (see figure 7), the difference between the soil saturation
 and saturation in the drainage network (i.e. 100%) is stronger for the base model than for the other two models. This leads
 to soil moisture fields more uniform for the SSF and SSF-DWF models than for the base model. This result is particularly
 425 observed for the Orbieu catchment.

Both the δ_1 and δ_2 spatial moments computed for the LDAS-Monde HU_{surf} are globally closer to 1 than when computed for
 the MARINE outputs. Indeed since the spatial resolution is the LDAS-Monde HU_{surf} is $2.5 \times 2.5 \text{ km}^2$, whereas it is 200×200
 m or 250×250 m for the MARINE simulations, the spatial variability of the LDAS-Monde HU_{surf} is lower than for the
 430 MARINE outputs. The δ_1 and δ_2 spatial moments computed for the CGLS SWI are very close to 1, with tiny variations. This
 can be explained not only by the spatial resolution coarser than for the MARINE outputs but also by the important amount of
 missing pixel in this data source, in particular for the Ardeche catchment. The computation of spatial moments for the CGLS
 SWI might not lead to robust conclusions.

Table 6. Kendall correlations between LDAS-Monde and MARINE soil moisture, on average per catchment, for each soil model.

Soil model	LDAS-Monde	Orbieu catchment			Ardeche catchment		
		Ev 02 2017	Ev 03 2017	Ev 10 2018	Ev 11 2018	Ev 03 2018	Ev 04 2019
Base	HU_{surf}	0.092	0.19	0.647	0.642	0.534	0.623
SSF	HU_{surf}	0.581	0.752	0.601	0.402	0.332	0.406
SSF-DWF	HU_{surf}	0.6	0.867	0.59	0.512	0.647	0.724

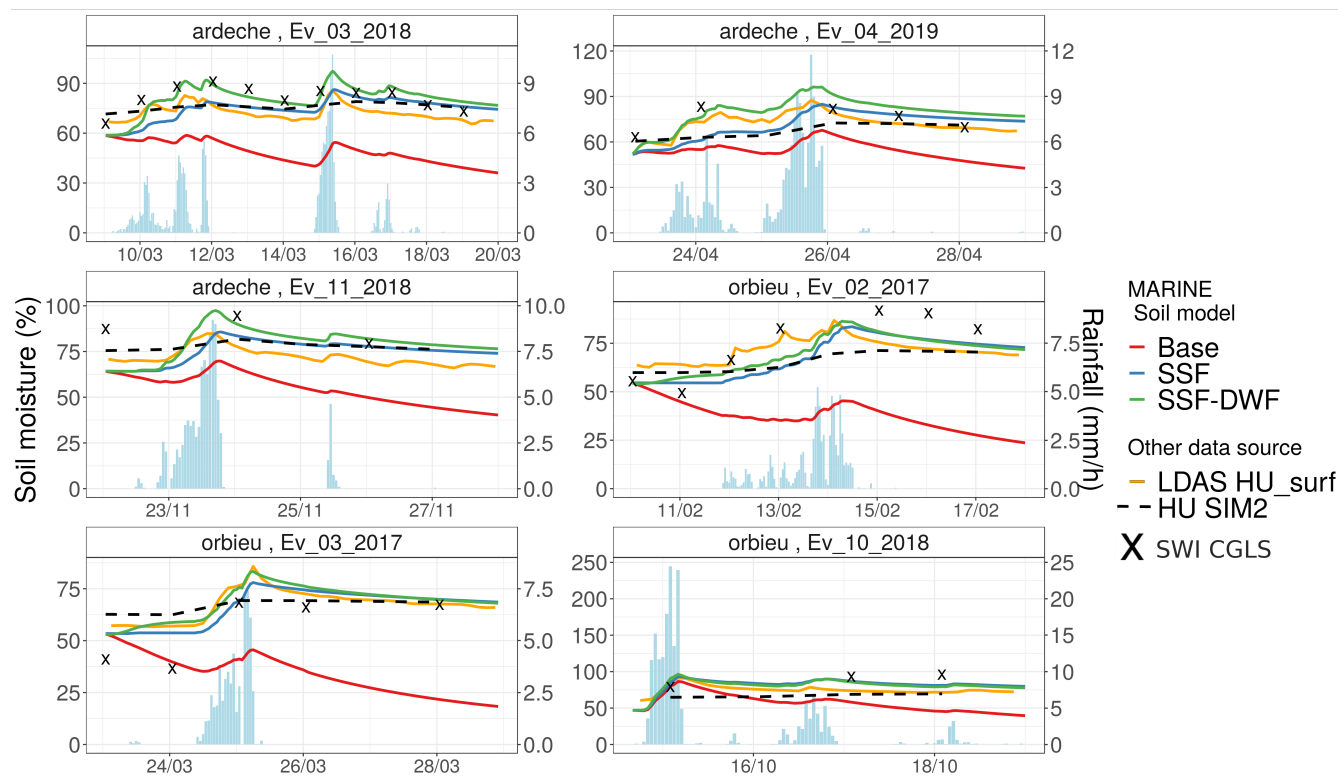


Figure 7. Soil moisture time series, on average per catchment, simulated with MARINE using the base, the SSF or the SSF-DWF models, and LDAS-Monde HU_{surf} and SWI CGLS values, in average per catchment.

4.2.2 Water content of the deep layer

435 Figure 11 presents the soil moisture simulated for the deep layer with the SSF-DWF model, together with the LDAS-Monde HU_{deep} time series, on average per catchment. The piezometric levels recorded at the measurement point of the ADES network for each catchment are also represented on this figure. Table 7 presents the Kendall correlations between the SSF-DWF deep layer moisture and the LDAS-Monde HU_{deep} .

Table 7. Kendall correlations between LDAS-Monde and MARINE deep layer moisture for the SSF-DW model.

		Orbieu catchment			Ardeche catchment		
Soil model	LDAS-Monde	Ev 02 2017	Ev 03 2017	Ev 10 2018	Ev 11 2018	Ev 03 2018	Ev 04 2019
SSF-DWF	HU_{deep}	-0.401	-0.258	-0.005	0.757	0.642	0.869

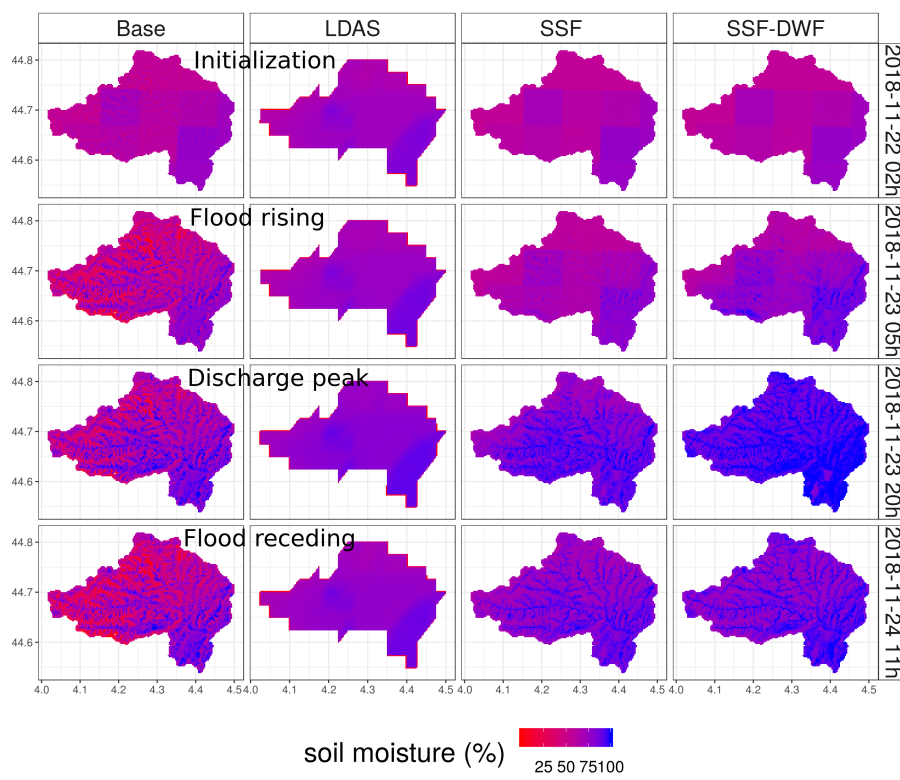


Figure 8. Maps of simulated soil moisture, for the example of the event of November, 2018 on the Ardeche catchment. MARINE simulation output with the base, the SSF and the SSF-DWF models are presented, and also the LDAS-Monde HU_{surf} maps. Four time steps of the simulation are considered: first time step of the run, one time step during the flow rise, the peak flow hour and one time step in the flow decreasing.

440 For the Ardeche catchment, the simulated deep layer moisture is well correlated with the LDAS-Monde HU_{deep} , with Kendall correlations between 6.4 and 8.7. This result enhance the reliability of the deep layer calibration in the SSF-DWF model for the Ardeche catchment. However, for this catchment, as the extend of the water table (1849 km^2) is large compared to the area impacted by extreme precipitation, the response of the piezometric level of the water table to the precipitation event is small. Then, these measurements can not be used to assess the simulated moisture of the deep layer at the catchment scale.

445

Furthermore, for the events over the Orbieu catchment, the simulated deep layer moisture appears not to be consistent with the LDAS-Monde HU_{deep} , in particular for the two events of February and March 2017. For the strong event of October 2018 on the Orbieu catchment, the sharp increasing of the deep soil moisture at the end of the rainfall event is observed in both the SSF-DWF model and in the LDAS-Monde HU_{deep} . The calibration of the deep layer in the SSF-DWF model for the Orbieu
 450 catchment leads to an emptying of deep soil faster than for the LDAS-Monde HU_{deep} variable. The simulation of the deep layer water content strongly depends on the calibration of the deep layer thickness, the deep layer porosity and the vertical and

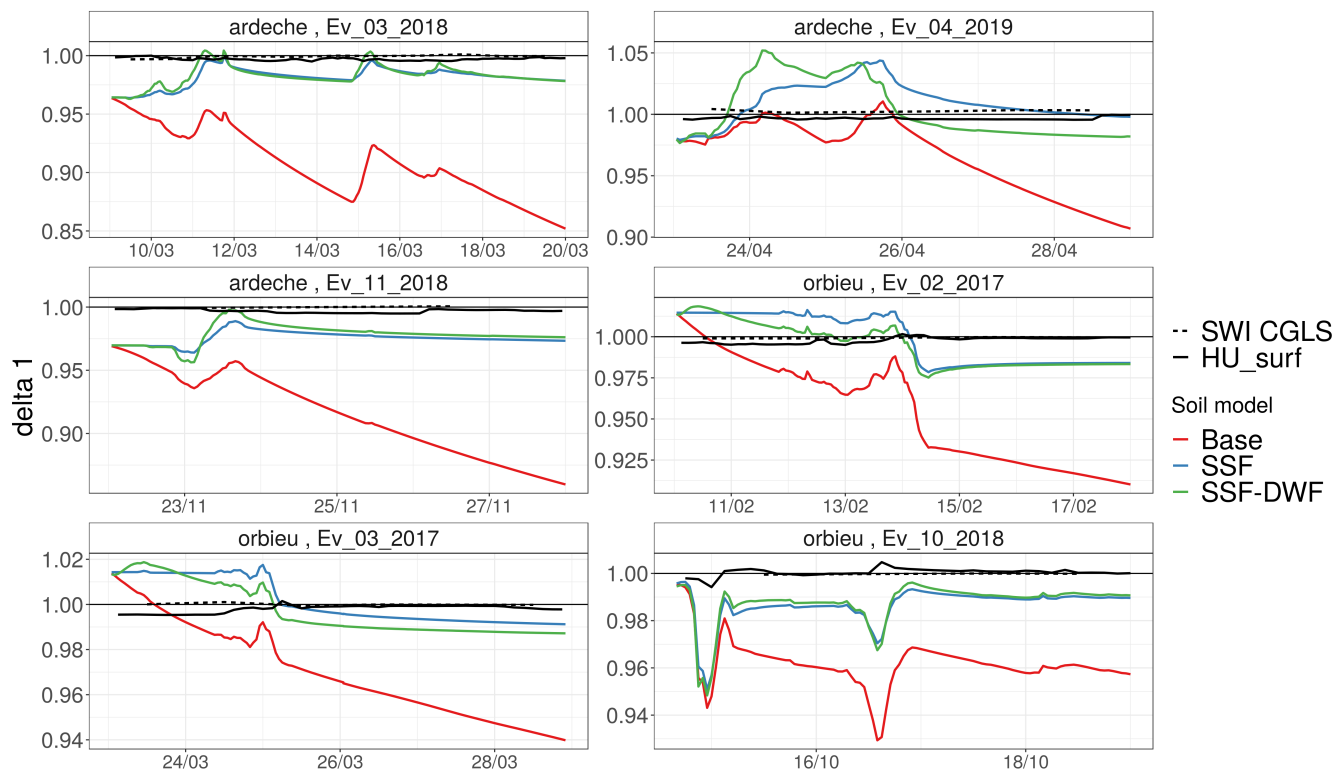


Figure 9. Time series of index δ_1 defined by Zocatelli et al. (2011) for the six events, computed for the soil moisture outputs for the BM, SSF and SSF-DWF models, and also for the LDAS-Monde HU_{surf} variable and the CGLS SWI.

lateral hydraulic conductivities in the deep layer. In this work, the vertical and lateral hydraulic conductivities of the deep layer are considered to be equal. Additional research regarding the deep layer calibration should be led.

455 For the Orbieu catchment, the extend of the water table (10 km^2) is smaller than for the Ardeche catchment, and the re-
 sponse of the piezometric level to precipitation is noticeable. However, its response strongly differs between the three studied
 events, depending on both the initial piezometric level and the amount of precipitation. For the strong event of October 2018,
 which started at with a low piezometric level, an increasing of the piezometry is observed immediately with the precipitation,
 whereas, for the small event of February 2017, the response of the water table is delayed of about two days. None of these
 460 behaviors are represented, neither in the SSF-DWF output, nor in the LDAS-Monde HU_{deep} product.

For the Ardeche catchment, the good correlations between the LDAS-Monde HU_{deep} and the deep layer moisture simu-
 lated with the SSF-DWF model highlights the consistency of this model for this catchment, and it corroborates the results of
 Douinot et al. (2018) which tend to show that this model is particularly suitable for discharge simulation in shale watershed.

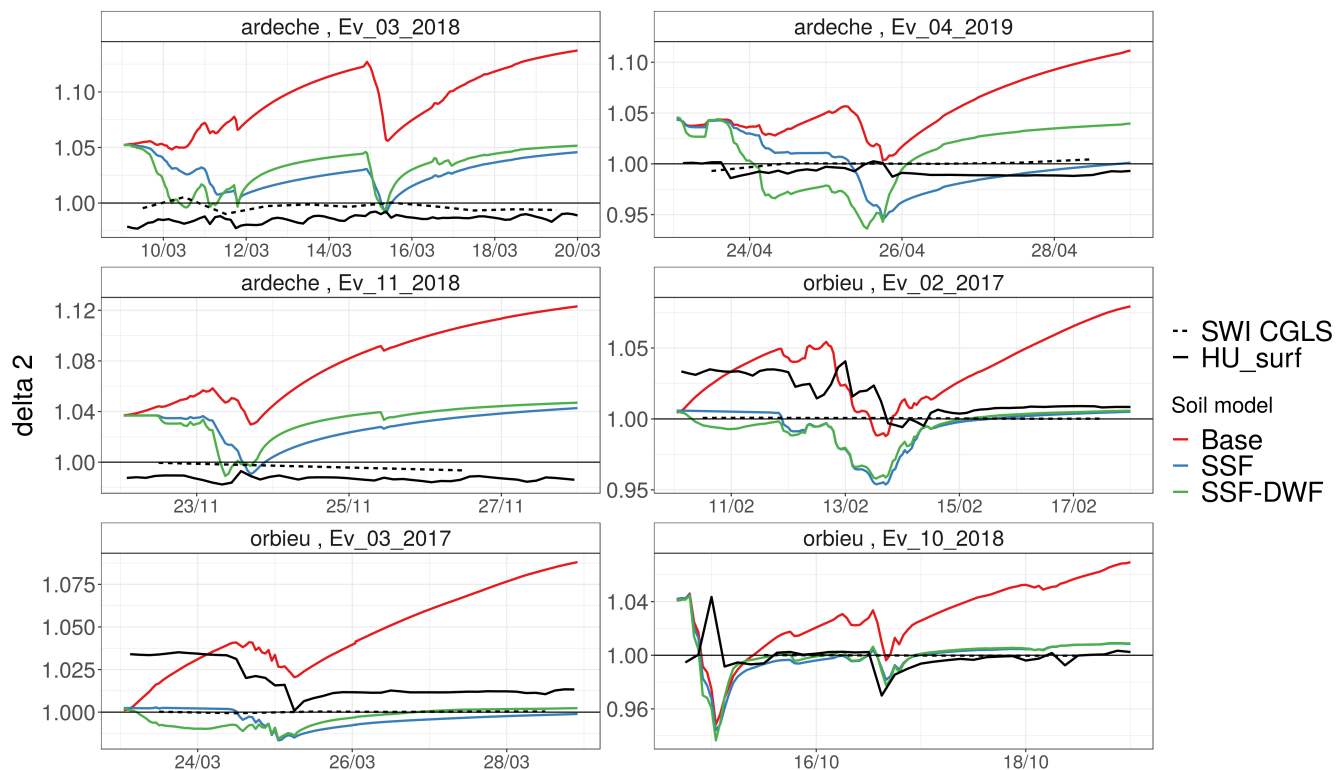


Figure 10. Time series of index $\delta 2$ defined by Zoccatelli et al. (2011) for the six events, computed for the soil moisture outputs for the BM, SSF and SSF-DWF models, and also for the LDAS-Monde HU_{surf} variable and the CGLS SWI.

465 Conversely, for the Orbieu catchment, the weak correlations between the LDAS-Monde HU_{deep} and the SSF-DWF model
 466 output corroborates the fact that this model seems less well suited for sedimentary catchments. These results illustrate the dif-
 467 ficulty to represent the hydrological dynamic of the deep soil layers, with limitation due to the lack of knowledge concerning
 468 the physical description of the subsurface water storage (Martin et al., 2004; Maréchal et al., 2013; Vannier et al., 2016).

5 Conclusions

470 The developments of the MARINE model presented by Douinot (2016) are exploited in this work. On the one hand, the trans-
 471 fers through the subsurface are computed based on the volumetric soil water content instead of the water height (SSF model).
 472 On the other hand, the soil column is divided into two layers, which represent respectively the upper soil layer and the deep
 473 weathered rocks (SSF-DWF model). These developments enhance the degree of refinement of the soil physics described in the
 474 model. The impacts of this representation of the subsurface on the water discharge are extensively studied by Douinot (2016).
 475 However, their influence on the spatial dynamic of soil saturation has not yet been explored. This paper aims to assess the

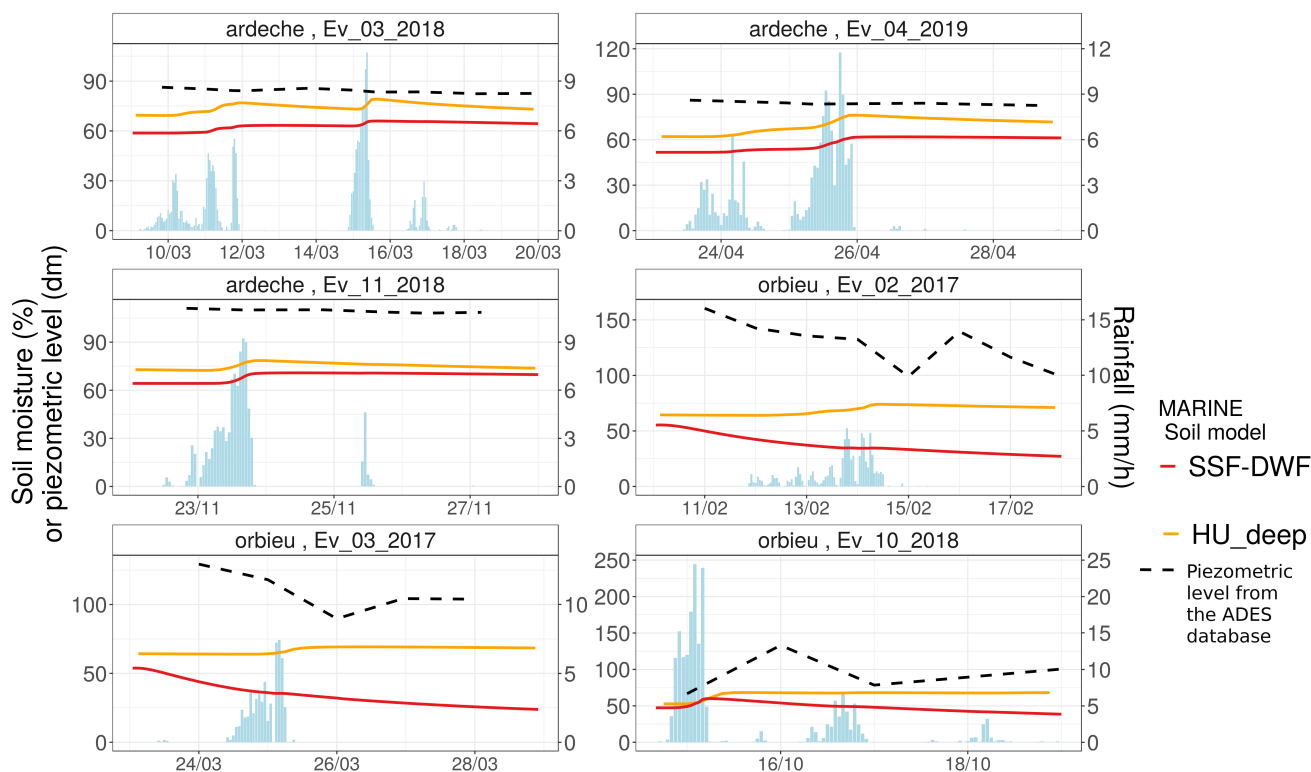


Figure 11. Soil moisture simulated for the deep layer with the SSF-DWF model, together with the LDAS-Monde HU_{deep} time series, on average per catchment.

performances of these developments for the representation of soil saturation during flash flood events.

The performances of the model are estimated with respect to several soil moisture products, either at the local scale or spatially extended: i) The gridded soil moisture product provided by the operational modeling chain SAFRAN-ISBA-MODCOU at the daily time step and at the 8-km resolution; ii) The gridded soil moisture product provided by the LDAS-Monde assimilation chain, based on the ISBA-a-gs land surface model and assimilating high resolution spatial remote sensing data, available at the hourly time step and at the 2.5-km resolution; iii) the upper soil moisture hourly measurements taken from the SMOS-MANIA observation network; iv) The Soil Water Index provided by the Copernicus Global Land Service (CGLS), derived from Sentinel1/C-band SAR and ASCAT satellite data, at the daily time step and at the kilometeric resolution. A comparative assessment of the various products based on remote imagery available for soil moisture in the literature is performed. This literature exploration of the data available for soil moisture description illustrates the difficulty to estimate surface soil moisture based on satellite data at small catchment scale ($\sim 100km^2$). Considering its satisfying data availability and its fine spatial resolution, the SWI product provided by CGLS is compared with the soil moisture simulated in MARINE. These products



represent valuable indicators of the spatio-temporal dynamics of soil moisture at various scales.

490

The case study is performed over two catchments located in the South of France, namely the Orbieu river catchment at the Lagrasse station and the Ardeche river catchment at the Vogue station, particularly impacted by flash flood mediterranean events. The study focuses on three flash flood events for each catchment, that occurred between February 2017 and April 2019. These six events present various characteristics, regarding mainly the structures of the pluviometric events and the soil moisture antecedent conditions. The MARINE flash flood model is set up following the calibrations provided by Garambois et al. (2015) for the Orbieu catchment and by Douinot (2016) for the Ardeche catchment. The ANTILOPE QPE data are used as hourly precipitation input for the MARINE model at the kilometric resolution. As the scope of this work is to assess the soil moisture simulation according to the physic considered in the soil models, the discharges simulated with the different models are considered as it is, and the calibrations are not further optimized. The comparison between the gridded soil moisture estimates and the local measurements of soil moisture provided by the SMOSMANIA network is performed through a spatial averaging of the gridded simulated values over a 1km^2 area around the measurement point. As the LDAS-Monde provides soil moisture values for 11 soil layers, these values are synthesized by three summary variables representing respectively the upper soil layer, the deep soil layer and the total soil column. The spatial distributions of soil moisture grids are quantitatively described through the definition of the spatial moments δ_1 and δ_2 .

505

The local comparison of the MARINE outputs for surface soil moisture with the SMOSMANIA measurements, as well as the comparison at the basin scale with the gridded LDAS-Monde and CGLS data lead to the same conclusions: soil moisture simulated with the base model significantly differs from the simulations using the SSF and the SSF-DWF models. When no precipitation happens, the soil layer empties faster with the base model, leading to a simulated soil moisture significantly lower with the base model than with the two other models. This behavior can be physically explained by the fact that, in the SSF and the SSF-DWF models, the lateral transfers are computed as a function of the volumic soil water gradients, whereas in the base model, they are computed as a function of the water height gradient. Indeed, since the water height gradient between two cells depends on the slope between the cells and the cells textures, water height gradients are larger than volumic soil water gradient when no precipitation happens. Consequently, lateral flows based on the water height gradients are larger than lateral flows based on the volumic soil water gradient. In addition, the dynamics as well as the amplitudes of the soil moisture simulated in the SSF model and for the upper layer in the SSF-DWF model are better correlated with both the SMOSMANIA measurements and the LDAS-Monde data than the outputs of the base model. Considering that the dynamics of the LDAS-Monde HU_{surf} is of satisfying accuracy, this assessment leads to the conclusion that the SSF-DWF model improves the simulation of the dynamics of the surface layer moisture, compared to both the SSF and the base models. This results appears to be particularly reliable, since it is observed both a the point measurement scale and at the catchment scale.

520

In the SSF-DWF model, the simulation of the moisture in the deep layer is also compared to LDAS-Monde moisture data provided for deeper layers, as well as local piezometric measurements available for each catchment. However, the simulation



of the deep layer water content strongly depends on the calibration of the deep layer thickness, the deep layer porosity and the
525 vertical and lateral hydraulic conductivities in the deep layer. These results illustrate the difficulty to represent the hydrological
dynamic of the deep soil layers, with limitation due to the lack of knowledge concerning the physical description of the subsur-
face water storage. Further conclusions concerning the simulation of deep soil moisture would then require an extensive work
to enhance the parametrization of the deep layer in the SSF-DWF model. In particular, the Height Above Nearest Drainage
(HAND) method (Nobre et al., 2011) would offer the opportunity to take into account the terrain physical characteristics in the
530 deep layer parametrization.

In conclusion, this work exposes that enhancing the degree of refinement of the soil physics for the representation of sub-
surface flow in the MARINE model appears to enhance the upper soil moisture simulation during flash floods, with respect to
both spatialized model outputs and satellite-based data, as well as with respect to local soil moisture measurements.

535 *Author contributions.* JE performed the model simulations and the comparison of the different products, and prepared the paper. HR su-
pervised the work. BB and CA provided the LDAS-Monde product and fed the discussion. AD designed and implemented the SSF and the
SSF-DWF models. All authors discussed the results and contributed to the text.

Competing interests. The authors declare that they have no conflict of interest.

Acknowledgements. This work was funded by the STAE-IRT Saint Exupery foundation, in the framework of the POMME-V project. The
540 THEAI-Land VHSR data are broadcast through the prism platform, available at www.theia-land.fr. The discharge measurements and the
SIM soil moisture data were provided by the French Service for Flood Prevision (SCHAPI). The precipitation data were provided by
MeteoFrance. The authors would like to thanks J.P. Wigneron, M. Zribi and N. Baghdadi for providing the SMOS-IC and THEAI-Land
VHSR data, respectively, and feeding the discussion on these products.



References

- 545 Adamovic, M., Branger, F., Braud, I., and Kralisch, S.: Development of a data-driven semi-distributed hydrological model for regional scale catchments prone to Mediterranean flash floods, *Journal of hydrology*, 541, 173–189, 2016.
- Al-Yaari, A., Wigneron, J.-P., Dorigo, W., Colliander, A., Pellarin, T., Hahn, S., Mialon, A., Richaume, P., Fernandez-Moran, R., Fan, L., et al.: Assessment and inter-comparison of recently developed/reprocessed microwave satellite soil moisture products using ISMN ground-based measurements, *Remote sensing of environment*, 224, 289–303, 2019.
- 550 Albergel, C., Rüdiger, C., Carrer, D., Calvet, J.-C., Fritz, N., Naeimi, V., Bartalis, Z., and Hasenauer, S.: An evaluation of ASCAT surface soil moisture products with in-situ observations in Southwestern France, *Hydrology and Earth System Sciences*, 13, 115–124, 2009.
- Albergel, C., Munier, S., Leroux, D. J., Dewaele, H., Fairbairn, D., Barbu, A. L., Gelati, E., Dorigo, W., Faroux, S., Meurey, C., et al.: Sequential assimilation of satellite-derived vegetation and soil moisture products using SURFEX_v8. 0: LDAS-Monde assessment over the Euro-Mediterranean area, *Geoscientific Model Development*, 10, 3889, 2017.
- 555 Albergel, C., Munier, S., Bocher, A., Bonan, B., Zheng, Y., Draper, C., Leroux, D., and Calvet, J.-C.: LDAS-Monde Sequential Assimilation of Satellite Derived Observations Applied to the Contiguous US: An ERA-5 Driven Reanalysis of the Land Surface Variables, *Remote Sensing*, 10, 1627, 2018.
- Aune-Lundberg, L. and Strand, G.-H.: CORINE Land Cover 2006. The Norwegian CLC2006 project, Norsk institutt for skog og landskap, 2010.
- 560 Barbu, A., Calvet, J.-C., Mahfouf, J.-F., Albergel, C., and Lafont, S.: Assimilation of Soil Wetness Index and Leaf Area Index into the ISBA-A-gs land surface model: grassland case study, *Biogeosciences*, 8, 1971–1986, 2011.
- Bauer-Marschallinger, B., Freeman, V., Cao, S., Paulik, C., Schaufler, S., Stachl, T., Modanesi, S., Massari, C., Ciabatta, L., Brocca, L., et al.: Toward global soil moisture monitoring with Sentinel-1: Harnessing assets and overcoming obstacles, *IEEE Transactions on Geoscience and Remote Sensing*, 57, 520–539, 2018a.
- 565 Bauer-Marschallinger, B., Paulik, C., Hochstöger, S., Mistelbauer, T., Modanesi, S., Ciabatta, L., Massari, C., Brocca, L., and Wagner, W.: Soil moisture from fusion of scatterometer and SAR: Closing the scale gap with temporal filtering, *Remote Sensing*, 10, 1030, 2018b.
- Berthet, L.: Prévion des crues au pas de temps horaire: pour une meilleure assimilation de l'information de débit dans un modèle hydrologique, Ph.D. thesis, 2010.
- Berthet, L., Andréassian, V., Perrin, C., and Javelle, P.: How crucial is it to account for the antecedent moisture conditions in flood forecasting?
- 570 Comparison of event-based and continuous approaches on 178 catchments, *Hydrology and Earth System Sciences*, 13, 819–831, 2009.
- Bonan, B., Albergel, C., Napoly, A., Zheng, Y., Druel, A., Meurey, C., and Jean-Christophe, C.: An offline reanalysis of land surface variables forced by a kilometric scale NWP system, in preparation, 2020.
- Bouilloud, L., Chancibault, K., Vincendon, B., Ducrocq, V., Habets, F., Saulnier, G.-M., Anquetin, S., Martin, E., and Noilhan, J.: Coupling the ISBA land surface model and the TOPMODEL hydrological model for Mediterranean flash-flood forecasting: description, calibration, and validation, *Journal of Hydrometeorology*, 11, 315–333, 2010.
- 575 Calvet, J.-C., Noilhan, J., Roujean, J.-L., Bessemoulin, P., Cabelguenne, M., Olioso, A., and Wigneron, J.-P.: An interactive vegetation SVAT model tested against data from six contrasting sites, *Agricultural and Forest Meteorology*, 92, 73–95, 1998.
- Calvet, J.-C., Fritz, N., Froissard, F., Suquia, D., Petitpa, A., and Pignat, B.: In situ soil moisture observations for the CAL/VAL of SMOS: The SMOSMANIA network, in: 2007 IEEE International Geoscience and Remote Sensing Symposium, pp. 1196–1199, IEEE, 2007.



- 580 Champeaux, J.-L., Dupuy, P., Laurantin, O., Soulan, I., Tabary, P., and Soubeyroux, J.-M.: Les mesures de précipitations et l'estimation des lames d'eau à Météo-France: état de l'art et perspectives, *La Houille Blanche*, pp. 28–34, 2009.
- Decharme, B., Boone, A., Delire, C., and Noilhan, J.: Local evaluation of the Interaction between Soil Biosphere Atmosphere soil multilayer diffusion scheme using four pedotransfer functions, *Journal of Geophysical Research: Atmospheres*, 116, 2011.
- Dewaele, H., Munier, S., Albergel, C., Planque, C., Laanaia, N., Carrer, D., and Calvet, J.-C.: Parameter optimisation for a better representation of drought by LSMs: inverse modelling vs. sequential data assimilation, *Hydrology and Earth System Sciences*, 21, 4861, 2017.
- 585 Dong, J., Crow, W. T., Tobin, K. J., Cosh, M. H., Bosch, D. D., Starks, P. J., Seyfried, M., and Collins, C. H.: Comparison of microwave remote sensing and land surface modeling for surface soil moisture climatology estimation, *Remote Sensing of Environment*, 242, 111 756, 2020.
- Dorigo, W., Gruber, A., De Jeu, R., Wagner, W., Stacke, T., Loew, A., Albergel, C., Brocca, L., Chung, D., Parinussa, R., et al.: Evaluation of the ESA CCI soil moisture product using ground-based observations, *Remote Sensing of Environment*, 162, 380–395, 2015.
- 590 Dorigo, W., Wagner, W., Albergel, C., Albrecht, F., Balsamo, G., Brocca, L., Chung, D., Ertl, M., Forkel, M., Gruber, A., et al.: ESA CCI Soil Moisture for improved Earth system understanding: State-of-the art and future directions, *Remote Sensing of Environment*, 203, 185–215, 2017.
- Douinot, A.: Analyse des processus d'écoulement lors de crues à cinétique rapide sur l'arc méditerranéen, Ph.D. thesis, <http://www.theses.fr/2016TOU30265>, thèse de doctorat dirigée par Dartus, Denis Hydrologie Toulouse 3 2016, 2016.
- 595 Douinot, A., Roux, H., and Dartus, D.: Modelling errors calculation adapted to rainfall–Runoff model user expectations and discharge data uncertainties, *Environmental Modelling & Software*, 90, 157–166, 2017.
- Douinot, A., Roux, H., Garambois, P.-A., and Dartus, D.: Using a multi-hypothesis framework to improve the understanding of flow dynamics during flash floods, *Hydrology and Earth System Sciences*, 22, 5317–5340, 2018.
- 600 Edouard, S., Vincendon, B., and Ducrocq, V.: Ensemble-based flash-flood modelling: Taking into account hydrodynamic parameters and initial soil moisture uncertainties, *Journal of Hydrology*, 560, 480–494, 2018.
- El Hajj, M., Baghdadi, N., Zribi, M., and Bazzi, H.: Synergic use of Sentinel-1 and Sentinel-2 images for operational soil moisture mapping at high spatial resolution over agricultural areas, *Remote Sensing*, 9, 1292, 2017.
- Fairbairn, D., Barbu, A., Napoly, A., Albergel, C., Mahfouf, J.-F., and Calvet, J.-C.: The effect of satellite-derived surface soil moisture and leaf area index land data assimilation on streamflow simulations over France, *Hydrology and Earth System Sciences*, 21, 2015–2033, 2017.
- 605 Fernandez-Moran, R., Al-Yaari, A., Mialon, A., Mahmoodi, A., Al Bitar, A., De Lannoy, G., Rodriguez-Fernandez, N., Lopez-Baeza, E., Kerr, Y., and Wigneron, J.-P.: SMOS-IC: An alternative SMOS soil moisture and vegetation optical depth product, *Remote Sensing*, 9, 457, 2017.
- 610 Fuamba, M., Branger, F., Braud, I., Batchabani, E., Sanzana, P., Sarrazin, B., and Jankowfsky, S.: Value of distributed water level and soil moisture data in the evaluation of a distributed hydrological model: Application to the PUMMA model in the Mercier catchment (6.6 km²) in France, *Journal of hydrology*, 569, 753–770, 2019.
- Garambois, P.-A.: Etude régionale des crues éclair de l'arc méditerranéen français. Elaboration de méthodologies de transfert à des bassins versants non jaugés, Ph.D. thesis, 2012.
- 615 Garambois, P.-A., Roux, H., Larnier, K., Labat, D., and Dartus, D.: Parameter regionalization for a process-oriented distributed model dedicated to flash floods, *Journal of Hydrology*, 525, 383–399, 2015.



- Garambois, P.-A., Douinot, A., Roux, H., and Dartus, D.: Méthodes de régionalisation pour un modèle pluie-débit distribué et à base physique dédié aux crues éclair, *La Houille Blanche*, pp. 71–77, 2016.
- Gaume, E., Bain, V., Bernardara, P., Newinger, O., Barbuc, M., Bateman, A., Blaškovičová, L., Blöschl, G., Borga, M., Dumitrescu, A., et al.:
620 A compilation of data on European flash floods, *Journal of Hydrology*, 367, 70–78, 2009.
- Habets, F., Boone, A., Champeaux, J.-L., Etchevers, P., Franchisteguy, L., Leblois, E., Ledoux, E., Le Moigne, P., Martin, E., Morel, S., et al.:
The SAFRAN-ISBA-MODCOU hydrometeorological model applied over France, *Journal of Geophysical Research: Atmospheres*, 113,
2008.
- IPCC: Climate change 2014, IPCC Working Group II, 2014.
- 625 Leroux, D., Calvet, J.-C., Munier, S., and Albergel, C.: Using Satellite-Derived Vegetation Products to Evaluate LDAS-Monde over the
Euro-Mediterranean Area, *Remote Sensing*, 10, 1199, 2018.
- Li, X., Al-Yaari, A., Schwank, M., Fan, L., Frappart, F., Swenson, J., and Wigneron, J.-P.: Compared performances of SMOS-IC soil moisture
and vegetation optical depth retrievals based on Tau-Omega and Two-Stream microwave emission models, *Remote Sensing of Environ-*
ment, 236, 111 502, 2020.
- 630 Lovat, A., Vincendon, B., et al.: Assessing the impact of resolution and soil datasets on flash-flood modelling, *Hydrology and Earth System
Sciences*, 23, 1801–1818, 2019.
- Manus, C., Anquetin, S., Braud, I., Vandervaere, J., Creutin, J. D., Viallet, P., and Gaume, E.: A modeling approach to assess the hydrological
response of small mediterranean catchments to the variability of soil characteristics in a context of extreme events, 2009.
- Maréchal, D., Ayral, P.-A., Bailly, J.-S., Puech, C., and Sauvagnargues-Lesage, S.: Sur l'origine morphologique des écoulements par l'analyse
635 d'observations hydrologiques distribuées. Application à deux bassins versants cévenols (Gard, France), *Géomorphologie: relief, processus,
environnement*, 19, 47–62, 2013.
- Martin, F., Martin, C., Lavabre, J., and Folton, N.: Fonctionnement hydrologique des bassins versants de roches métamorphiques: exemple
du bassin versant des Maurets (massif des Maures, Var, France), 2004.
- Masson, V., Le Moigne, P., Martin, E., Faroux, S., Alias, A., Alkama, R., Belamari, S., Barbu, A., Boone, A., Bouyssel, F., Brousseau, P.,
640 Brun, E., Calvet, J. C., Carrer, D., Decharme, B., Delire, C., Donier, S., Essaouini, K., Gibelin, A. L., Giordani, H., Habets, F., Jidane,
M., Kerdraon, G., Kourzeneva, E., Lafaysse, M., Lafont, S., Brossier, C. L., Lemonsu, A., Mahfouf, J. F., Marguinaud, P., Mokhtari,
M., Morin, S., Pigeon, G., Salgado, R., Seity, Y., Taillefer, F., Tanguy, G., Tulet, P., Vincendon, B., Vionnet, V., and Voldoire, A.: The
SURFEXv7.2 land and ocean surface platform for coupled or offline simulation of earth surface variables and fluxes, *GEOSCIENTIFIC
MODEL DEVELOPMENT*, 6, 929–960, <https://doi.org/10.5194/gmd-6-929-2013>, 2013.
- 645 Nobre, A. D., Cuartas, L. A., Hodnett, M., Rennó, C. D., Rodrigues, G., Silveira, A., and Saleska, S.: Height Above the Nearest Drainage—a
hydrologically relevant new terrain model, *Journal of Hydrology*, 404, 13–29, 2011.
- Noilhan, J. and Mahfouf, J.-F.: The ISBA land surface parameterisation scheme, *Global and planetary Change*, 13, 145–159, 1996.
- Noilhan, J. and Planton, S.: A simple parameterization of land surface processes for meteorological models, *Monthly weather review*, 117,
536–549, 1989.
- 650 Parrens, M., Zakharova, E., Lafont, S., Calvet, J.-C., Kerr, Y., Wagner, W., and Wigneron, J.-P.: Comparing soil moisture retrievals from
SMOS and ASCAT over France, *Hydrology and Earth System Sciences*, 16, 423–440, 2012.
- Payrastre, O., Gaume, E., and Andrieu, H.: Usefulness of historical information for flood frequency analyses: Developments based on a case
study, *Water resources research*, 47, 2011.



- Perrin, C., Michel, C., and Andréassian, V.: Improvement of a parsimonious model for streamflow simulation, *Journal of hydrology*, 279, 275–289, 2003.
- 655
- Robbez-Masson, J., Barthes, J., LEGROS, J., et al.: Bases de données pédologiques et systèmes d'informations géographiques. L'exemple de la région Languedoc-Roussillon., *Forêt méditerranéenne*, 2000.
- Roux, H., Labat, D., Garambois, P.-A., Maubourguet, M.-M., Chorda, J., and Dartus, D.: A physically-based parsimonious hydrological model for flash floods in Mediterranean catchments, *Natural Hazards and Earth System Sciences*, 11, 2567–2582, 2011.
- 660
- Ruin, I., Lutoff, C., Boudevillain, B., Creutin, J.-D., Anquetin, S., Rojo, M. B., Boissier, L., Bonnifait, L., Borga, M., Colbeau-Justin, L., et al.: Social and Hydrological responses to extreme precipitations: an interdisciplinary strategy for postflood investigation, *Weather, climate, and society*, 6, 135–153, 2014.
- Spaargaren, O.: Report on the classification into FAO-Unesco soil units of profiles selected from the NRCS pedon data base for IGBP-DIS, 1995.
- 665
- Suárez-Almiñana, S., Solera, A., Madrigal, J., Andreu, J., and Paredes-Arquiola, J.: Methodology based on modelling processes and the characterisation of natural flows for risk assessment and water management under the influence of climate change, *Hydrol. Earth Syst. Sci. Discuss.*, <https://doi.org/10.5194/hess-2019-496>, <https://www.hydrol-earth-syst-sci-discuss.net/hess-2019-496/>, 2019.
- Tabary, P.: The new French operational radar rainfall product. Part I: Methodology, *Weather and forecasting*, 22, 393–408, 2007.
- Tramblay, Y., Bouvier, C., Martin, C., Didon-Lescot, J.-F., Todorovik, D., and Domergue, J.-M.: Assessment of initial soil moisture conditions for event-based rainfall–runoff modelling, *Journal of Hydrology*, 387, 176–187, 2010.
- 670
- Vannier, O., Braud, I., and Anquetin, S.: Regional estimation of catchment-scale soil properties by means of streamflow recession analysis for use in distributed hydrological models, *Hydrological Processes*, 28, 6276–6291, 2014.
- Vannier, O., Anquetin, S., and Braud, I.: Investigating the role of geology in the hydrological response of Mediterranean catchments prone to flash-floods: Regional modelling study and process understanding, *Journal of Hydrology*, 541, 158–172, 2016.
- 675
- Vincendon, B., Ducrocq, V., Saulnier, G.-M., Bouilloud, L., Chancibault, K., Habets, F., and Noilhan, J.: Benefit of coupling the ISBA land surface model with a TOPMODEL hydrological model version dedicated to Mediterranean flash-floods, *Journal of Hydrology*, 394, 256–266, 2010.
- Wagner, W., Dorigo, W., de Jeu, R., Fernandez, D., Benveniste, J., Haas, E., Ertl, M., et al.: Fusion of active and passive microwave observations to create an essential climate variable data record on soil moisture, *ISPRS Annals of the Photogrammetry, Remote Sensing and Spatial Information Sciences (ISPRS Annals)*, 7, 315–321, 2012.
- 680
- Wigneron, J.-P., Kerr, Y., Waldteufel, P., Saleh, K., Escorihuela, M.-J., Richaume, P., Ferrazzoli, P., De Rosnay, P., Gurney, R., Calvet, J.-C., et al.: L-band microwave emission of the biosphere (L-MEB) model: Description and calibration against experimental data sets over crop fields, *Remote Sensing of Environment*, 107, 639–655, 2007.
- Zocatelli, D., Borga, M., Viglione, A., Chirico, G., and Blöschl, G.: Spatial moments of catchment rainfall: rainfall spatial organisation, basin morphology, and flood response, *Hydrology and Earth System Sciences*, 15, 3767–3783, 2011.
- 685